Precambrian Research 398 (2023) 107121

Contents lists available at ScienceDirect

Precambrian Research

journal homepage: www.elsevier.com/locate/precamres

Growth faults and avalanches: Reconstructing Paleoarchean basins in the Pilbara and Kaapvaal cratons

Wouter Nijman [a,*], Sjoukje T. de Vries [a], Armelle Kloppenburg [b]

[a] Dept. of Earth Sciences, Faculty of Geosciences, Utrecht University, Princetonlaan 8a, 3584 CS Utrecht, The Netherlands
[b] 4DGeo Applied Structural Geology, Daal en Bergselaan 80, 2565 AH The Hague, The Netherlands

ARTICLE INFO

Keywords:
Paleoarchean extension tectonics
Archean volcano-sedimentary complexes
Archean basin analysis
Basin margins
Growth faults
Slope collapse
Pilbara
Coonterunah Subgroup
Barberton greenstone belt
Buck Reef Chert

ABSTRACT

Four new volcano-sedimentary complexes (VSC's), respectively c. 3510, 3460, 3430, and 3320 Ma old, are identified in the East Strelley, Coongan, and Kelly belts of the East Pilbara craton and compared with the extraordinarily complete c. 3450 Ma Buck Reef-VSC in the southern African Kaapvaal craton. The VSC's reveal an intricate relationship between volcanic deposition, sedimentation, development of syndepositional fault arrays, both extensional and contractional, and magmatism. The geometry and kinematics of these fault systems were analyzed after restoring the tilt of the stratigraphic sequences back to the depositional horizontal. The growth fault arrays are interpreted to have been generated by lack of lateral support of depositional basin margin prisms as known from present-day deltas and passive margins. This 'basin margin collapse' scenario for deformation and kinematics of the topmost section of the crust relies on topographic relief combined with vertical crustal oscillation. The relationship between supracrustal collapse and coeval deformation on deeper-seated detachments within the basement of the Pilbara remains as yet unsolved.

The restoration corroborates the (semi-)circular basin architecture we proposed in 2017, which preceded, and is unrelated to, the present-day configuration of granitoid complexes and greenstone belts. The new findings also assess an early, syndepositional presence of the east–west Warrawoona Lineament as a major dividing line of as yet unknown structural character between two areas of basin superposition.

For the Coonterunah Subgroup a multistorey architecture is established: the Table Top/Coucal-VSC with its near-water level chert top is overlain by regularly bedded Double Bar Basalt. The ensemble is truncated by the newly introduced tectono-stratigraphic Bergamina Unit, interpreted as a mega-avalanche emplaced somewhere between 3496 and 3466 Ma, possibly time-equivalent to the Duffer Fm.

The crustal depths of the detachments below the (water-level) tops of all VSC's identified, in other words the thicknesses of the VSC's, are used as proxy for determining minimum basin centre depths ranging from 1000 to 3800 m. The greatest depth was reached in the North and South Coongan Basins, where voluminous bimodal volcanism of the Duffer Fm, maximum subsidence and deposition rates resulted in maximum basin margin instability.

1. Introduction

1.1. Objective

The topic of this article is syndepositional deformation in Paleoarchean parts of eastern Pilbara greenstone belts that until now have not been investigated in detail. We also discuss its implication for the geometry and character of basins at that time. The key areas of focus of this paper are the Kelly and Coongan greenstone belts[1], and the stratigraphically oldest Coonterunah Subgroup in the East Strelley greenstone belt (Fig. 1). This study builds on previous publications in the Earth's Earliest Basins project (e.g. Nijman et al. 2017, and references therein), in which supracrustal structures related to depositional mass imbalance, basin margin collapse, and slope failure were recognized as the main style of deformation during deposition in Paleoarchean greenstone belts of the Pilbara and Kaapvaal cratons. In this contribution, we expand on those studies. The basin setting we have proposed for these structures is quite different from Phanerozoic analogues (cf.

* Corresponding author.
E-mail address: w.nijman@uu.nl (W. Nijman).

[1] Greenstone belt nomenclature according to *Fig. 8* in Hickman (2021).

https://doi.org/10.1016/j.precamres.2023.107121
Received 1 August 2022; Received in revised form 6 June 2023; Accepted 6 June 2023
Available online 21 October 2023

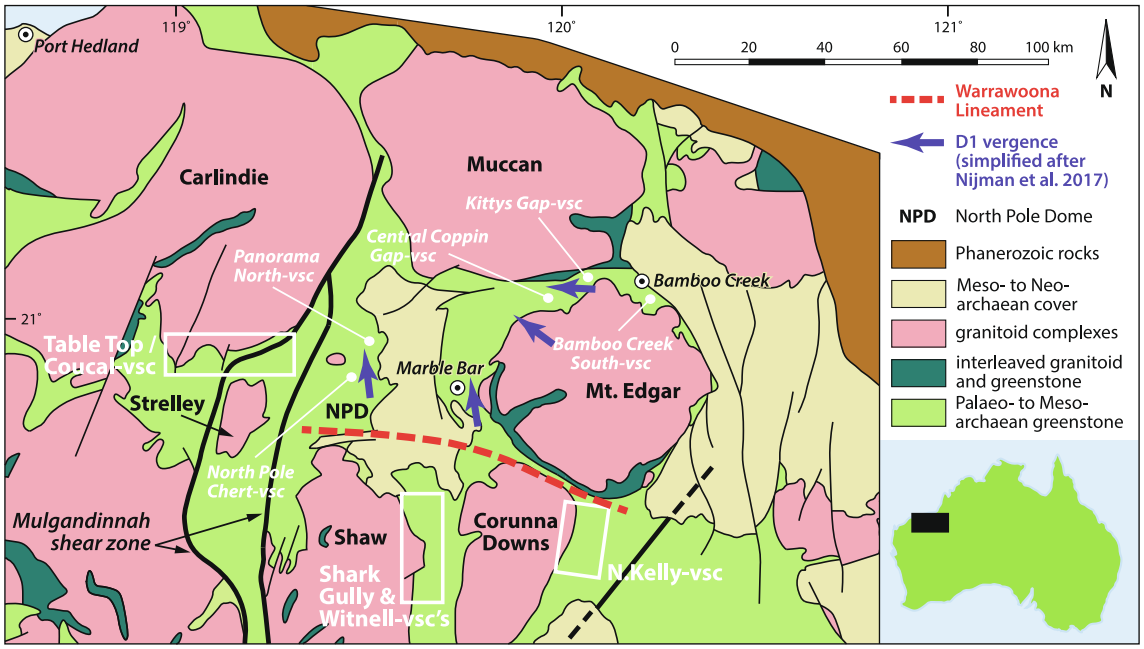

Fig. 1. Index map of the east Pilbara, with position of volcano-sedimentary complexes, Warrawoona Lineament, and Mulgandinnah Shear Zone. The depicted D1 vergences are those resulting from our previous research in the area north of the Warrawoona Lineament.

Hamilton 2007, 2019). Possibly more appropriate for the early Archean, we compared the basin style, in size and shape, with the one interpreted for basins on other terrestrial planets, like the ring-faulted coronae of Venus (Nijman and De Vries 2004).

The normal fault arrays and mega-avalanche here described extend our understanding of the basin configuration of the east Pilbara between 3.53 and 3.13 Ga. We compare them with the fault array of similar age in the Buck Reef volcano-sedimentary complex in the South African sector of the Barberton greenstone belt, previously mapped and analyzed by us in detail (e.g. De Vries et al. 2006b), but here restored to its syndepositional geometry.

The outcome of the current study underpins gravitational collapse as the oldest recognizable upper crustal expression of geodynamic processes over a period of at least 200 million year forming these Paleoarchean greenstone belts. It explains the integrated observations of both extensional and linked contractional faults, the regional pattern of vergences and a facies distribution that corresponds to that setting. To what extent growth fault arrays can be used as a proxy for basin depth will also be discussed.

1.2. Supracrustal collapse

The Paleoarchean extensional structures described in this article have many features in common with those found along Phanerozoic passive continental margins and modern-day deltas. These purely gravitational structures are well-imaged by 2D and 3D seismic datasets (many references in McClay and Hammerstein 2020) around the globe, particularly in those thought of hosting a successful petroleum system. An early example of submarine extensional collapse faulting is given by Garfunkel (1984) from the Plio-Pleistocene (<5.3 Ma) eastern Mediterranean shelf where 60° basinward-dipping extensional growth faults affected the shelf over an area of >1000 sq.km. Research by Shell in the Niger Delta (e.g. Mandl and Crans 1981) led to a better understanding of growth faulting and surficial slumping merely due to sedimentation (see also Hooper et al. 2002; Restrepo-Pace 2020). In deltas, overpressuring of shale by loading is the leading mechanism for the formation of collapse structures. Collapse in passive margins, however, formed by detachment over incompetent underlying salt layers (e.g., studies of West African shelf by Dupré et al. 2007; Anqing et al. 2013; Cramez and Jackson 2000; and from the Brazilian margin: Tamara et al. 2020; Fernandez et al. 2020). The evaporites were deposited in (half)grabens that developed during the aftermath of initial rifting preceding the forming of the passive margins (e.g. Marton et al. 2000; Rowan et al. 2012). Listric fault arrays below the salt-based collapse structures originated during that early rifting stage.

To distinguish collapse faults from extensional rift faults requires analysis of the larger context. Peel (2014) in a paper on deformation of passive margins, aiming at quantifying the influence of crustal spreading vs. depositional imbalance, makes the following introductory statement: *(his page 126) "Deformation of sedimentary sequences by gravitational tectonics occurs in most of the world's passive margins, and also in other planets. Gravitational deformation commonly consists of thin-skinned linked systems, in which a body of sediments is translated basinwards, accommodated by extension in its updip portion, and contraction in the downdip region. This can occur on a range of scales, from small failures affecting a few meters of sediment to giant systems affecting bodies 10-s of km thick and 100s of km long in the transport direction"*. Hence, coeval extension and contraction in a single system identifies it as being due to mass imbalance (cf. Oliveira et al. 2012)

Whereas the rift and post-rift collapse extensional fault systems are often related in space (*i.e.* the older faults may influence the location and spacing of the younger faults: Dooley et al. 2020), their driving forces are different. Collapse faulting is purely gravitationally controlled, with topographic build-up and lack of lateral support leading to failure. The fault size, geometry and association with rollover anticlines (Mauduit and Brun 1998) depend further on the amount and inhomogeneity of material deposited, in other words on the facies distribution and resulting relative strength of the layers involved. Relatively weak stratigraphic layers, whether in the sedimentary prisms of present-day passive margins or in the completely different volcanic rock sequences of the Paleoarchean basins, may form detachments at levels at or above the basin floor (Jarrige 1992), an argument used in this article when dealing with basin depth.

A tectonic-scale cause (other than rifting) for variation of tilt of basin margins contributing to excess gravitational potential energy is proposed by Hodgson and Rodriguez (2017). Shelf instability and change of slope gradient are considered to be caused by repeated rise and fall (oscillation) of the crust created by plate drift over isolated mantle

plumes arising from a major mantle convection cell *("lateral basin migration over the irregular asthenosphere" [their p. 97])*. These workers describe gravitational collapse structures *(catastrophic collapse mass-transport complexes [MTCs] and slowly forming megaslides [their p. 97])* in the Cretaceous-Tertiary shelf sequence of the Orange River Basin (Namibia and South Africa). Therefore, they relate observed superposition of gravitational detachment complexes with crustal oscillation.

Distinguishing rift-related or deeper-seated extensional faults from uppermost crustal collapse-related ones has therefore implications for the discussion about Paleoarchaean tectonics. Listric normal faulting also occurs in relation to metamorphic core complexes formed during crustal extension, directly or indirectly controlled by plate motion. The question whether surficial collapse tectonics in our examples was related to core complexes will be addressed as well.

1.3. Context of this study within the Earth's Earliest Basins project investigations.

Nijman et al. (2017; and further references therein) argued that syndepositional listric normal fault arrays in the Paleoarchean greenstone belts of the east Pilbara represent the first and long-lasting extensional deformation phase (D1), followed by a phase of crustal shortening (D2). These two phases preceded the 3.19–2.90 Ga development of the dome-and-belt architecture (D3) so characteristic of the present-day outcrop pattern in birds-eye view. The D1 normal fault arrays are intraformational because they syndepositionally deform shallowing-up volcano-sedimentary sequences and are underlain and overlain by formations unaffected by that deformation.

In this article, we use the term *volcano-sedimentary complex* ("VSC") as: *"A rock sequence grading from mafic via felsic volcanic rock into sedimentary chert, affected by a linked extensional to contractional growth fault array"*. This is a fine-tuning of the definition used in Nijman et al. (2017) and restricts the generic use of the term. As will be shown in this article, some elements may be missing in field observations: the relative amount of mafic vs felsic content may vary, and the contractional frontal part of a fault array may be absent or, if present, cannot be linked to the extensional rear.

In our previous studies, stepwise restoration of D3 and D2 structures allowed inspection of the D1 extensional structures in their original orientation. The restoration first removed the effects of the < 3.2 Ga D3 doming by back rotation of the dip angle of the bedding around the current strike. Between 3.31 and 3.19 Ga, D2 thrusts and overthrusts with NW-dipping foliation appeared to be controlled by NW-SE crustal shortening (Nijman et al. 2017: *their fig. 8)*. The southeast vergence of D2 structures, however, is only observed in the area north of the Warrawoona Lineament, initially recognized and named Central Warrawoona Shear Zone by Zegers (1996). South of this lineament the D2 vergence is opposite, westward, rendering the Warrawoona Lineament a dextral transfer fault, consistent with structural field observations (Kloppenburg et al. 2001).

Removal of the effects of D2 deformation showed that in the Pilbara sector north of the lineament the vergence of the D1 growth fault systems gradually changes from due west in the northeastern Bamboo Creek area to due north in the central part of the North Pole Dome (Fig. 1; Nijman et al. 2017).

These studies have led us to interpret the listric normal fault arrays to not have resulted from *tangential* deep-crustal scale stresses but from collapse following uplift and, as such, to be primarily basin-margin instability-dependent (Nijman and De Vries 2004). Although similar to orogenic collapse, this process does not require orogenic crustal thickening. Neither should the basins be considered calderas as for instance suggested for the Dresser Fm by Caruso et al. (2021; cf. for sliding in a caldera Branney and Kokelaar 1994), but as much larger collapse structures, comparable to but at least twice the size of present-day supervolcanoes (e.g. the 35 by 100 km Toba caldera complex of Sumatra is the largest Quaternary supervolcano, Koulakov et al. 2016). Besides, none of the known supervolcanoes are fully basaltic (De Silva and Self 2022). In the Pilbara, in our proposed scenario (Nijman et al. 2017), the 3.46–3.45 Ga (D1) Paleoarchean basins, however, were generated in a predominantly basaltic volcanic environment, in which ring faults were used as felsic volcanic conduits only during their late stage. Underlying this unique crustal setting is melting of water-saturated basaltic slabs or flakes that sank to lower crustal levels, and as such contributed to generating the involved bimodal volcanism (Nijman and De Vries 2004). In this context, the term oscillation was used, not referring to recurrent crustal rise and fall due to plate motion over mantle plumes (see Section 1.2), but to eclogite dripping at the Moho as proposed in the plume lid model of Fisher and Gerya (2016). The latter is supposed to create an *intra*crustal plume causing supracrustal rise, a process repeating itself after sealing of the decaying hotspot (crustal fall) by a basin fill. This mechanism we applied to explain the basin superposition observed in the Pilbara (Nijman et al. 2017).

Building on conclusions of Bickle et al. (1980), Boulter et al. (1987), and Zegers (1996), and having observed the widespread evidence of thrust deformation in the Pilbara, we considered plate tectonics to have started in the Pilbara at 3.31 Ga, to become - until 3.19 Ga - the driving force for D2 regional crustal shortening (Nijman et al. 2017). The D2 compression was inferred to have initiated the instability which led to D3 crustal overturn of the mafic and felsic crustal components resulting in the characteristic dome-and-belt architecture.

It is significant to recognize that we don't know what these extensional structures at this upper-crustal level mean in terms of the interpretation of processes on the lithospheric scale and their driving forces. Studies of the lithospheric development in Archean cratons have focused on identifying tectonic processes that are either of a modern style (with active plate-tectonic interactions), or of a typical Archean style (passive, gravitational crustal overturn). In the eastern Pilbara, upper crustal extensional faults have been linked in time and place to magmatism, regional crustal extension, and development of mid-crustal horizontal detachments with unidirectional, not radial, transport direction (Split Rock Shear Zone: Zegers et al.1996; Mount Edgar Shear Zone: Kloppenburg 2003), active during deposition of the Duffer Fm and the Salgash Subgroup. These two publications expressed that the classic model of solid-state diapirism on the scale of individual granitoid complexes was insufficient to explain these structures, their structural pattern, or their kinematics. Any regional-scale concept of the setting in which the VSC's discussed below developed will have to explain the coeval development of the structures at mid-crustal level, at this moment, as we will see, a relationship that is as yet not fully understood. Even the notion of 'mid-crust' is equivocal as long as we do not know the composition, geothermal gradient, nor thickness of early Earth's crust.

1.4. Methods and scope

The present study is based on integration of new satellite imagery interpretation with information from the Utrecht University field data base and the recent set of 1:100 000 GSWA geologic map sheets with explanatory notes of the Pilbara by the Geological Survey of Western Australia. Satellite imagery is from Google Earth and was collected in 2011, 2013, 2014, 2015, 2017, and 2018. The interpretations are therefore based on combinations of images, not only on those presented in the figures and supplementary material. Satellite data gives valuable primary information about geometry and structure, which often cannot be observed from close-by in the field. Mostly, we use satellite data in combination with extensive field observations. In the current article, we also interpret satellite data in some areas where we have very limited

ground truthing, Pilbara and Barberton greenstone belts. With the generally subvertical orientation of bedding and structures, fault and fold patterns, where intraformational, are described as normal faults and thrusts as if they were in their original orientation before tilting. The presented satellite maps can therefore be read and interpreted as seismic cross-sections and are for that reason not oriented north-up but stratigraphically younging-up.

In this study we focus on:

- new satellite image interpretation, investigating the syndepositional character of the Coongan and eastern Kelly Belts of the Pilbara, previously reported to enclose extensional structures (Zegers 1996; Kloppenburg 2003)
- multistorey architecture of the oldest Pilbara rock sequence, the 3.5 Ga Coonterunah Subgroup (Buick et al. 1995), composed of an extensional growth fault array covered by basalt and the ensemble truncated by a newly recognized, internally structurally disorganized tectono-stratigraphic unit comparable to a submarine slide as described by Masson et al. (2006);
- restoration to depositional geometry of the Buck Reef volcano-sedimentary complex in the Barberton greenstone belt of South Africa, based on detailed maps edited at Utrecht University (Nijman and De Vries 2005);
- deduction of mass transport directions from vergences of the restored VSC's to constrain size and shape of associated basins;
- growth fault geometry and detachment depth as proxy for basin depth.

Chapters and several sections in this article begin with a summarizing paragraph.

2. The North Kelly volcano-sedimentary complex

In the northeastern Kelly Belt, the combination of structural and stratigraphic features characterizes the felsic volcanic rock sequence of the Panorama Formation capped by the Strelley Pool Chert (Fig. 2; satellite base map in Supplementary Fig. 2*) as a volcano-sedimentary complex (here named: *North Kelly-VSC*). In architecture and size, it is similar to the Kittys Gap-VSC (e.g. De Vries et al. 2006a, 2010; Westall et al. 2006), and because of its orientation it provides an important clue for the proposed basin configuration and syndepositional tectonic configuration of the east Pilbara.

Stratigraphy. Fig. 2 shows a 60−70° east-dipping sequence of felsic volcanoclastic rock (tuff, agglomerate and breccia) with intercalation of basalt, capped by chert and overlain by basalt. The sequence is situated in the northern part of the N-S striking Kelly Belt where the latter meets the E-W striking southern sector of the Marble Bar Belt (previously known as Warrawoona Belt). In the 1:100 000 GSWA maps of that area (sheet Nullagine, Bagas et al. 2004a; Bagas 2005; sheet Mount Edgar, Williams and Bagas 2004; Williams et al. 2007), the sequence is assigned to the Panorama Formation, Strelley Pool Chert *(further abbreviated: SP Chert*) and Euro Basalt. There is no evidence of an unconformity between the Panorama Fm and the SP Chert. The SP Chert hosts stromatolites in this area (Grey et al. 2012). In the Mount Edgar map sheet, the presence of the Panorama Fm is corroborated by four U-Pb zircon ages (Fig. 2) varying between 3435 (3433 ± 2) Ma and 3424 (3428 ± 4) Ma. This age range overlaps with that of the youngest occurrence of the Panorama Fm about 85 km northwestwards along the north flank of the North Pole Dome (3434 ± 5 Ma, Van Kranendonk 2000; Van Kranendonk et al. 2001). Formations older than the Panorama Fm, such as the Apex and Duffer Fms, are not exposed or absent because of non-deposition or stratigraphic truncation.

Structure. Faults, updip extinguishing against the undisturbed SP Chert (Fig. 2), are evidently listric; downdip they merge into bedding-parallel detachments while accommodating stepwise increases of thickness and back tilt of the hanging-wall sequences. Upwards convex arching of the stratification characteristic for rollover anticlines in extensional growth fault complexes is obvious (crests in Fig. 2 located [^{1}943^{76}205]and [^{1}933^{76}175])[2]. Stratigraphically upwards, the faults and their offset die out within the uppermost felsic unit in which the stratification becomes progressively flatter towards parallel with the final cover of SP Chert.

Within the upper felsic unit [^{1}940^{76}190] and just above the sole detachment of the listric faults [^{1}927^{76}200], intraformational folds with axial planes parallel to bedding have the very characteristic shape of slump folds, in places recumbent and isoclinal with thick hinges, and with a tendency to chaotization [^{1}935^{76}165]. They are restricted to particular intervals of the sequence between undisturbed beds.

Veins and intrusions. Vein systems do occur, such as chert veins ascending into the SP Chert. Younger dolerite dykes cross-cut both the VSC-sequence and the overlying basalt. Along one of the normal faults near the detachment plane, now-serpentinized peridotite intruded into the VSC-sequence (Fig. 2: [^{1}930^{76}210], map legend: "ADA-mark" from Williams and Bagas 2004). The greenstone belt, as a whole, has been intruded by 3311 Ma monzogranites of the Corunna Downs granitoid complex.

Interpretation. We interpret the deformation to be intraformational, fault action being almost exclusively restricted to the North Kelly felsic sequence below its undisturbed cap of SP Chert. The listric faults with roll-over anticline, back tilt, and associated slumps characterize the structure of the North Kelly-VSC as a syndepositional growth fault array. Using the SP Chert as originally horizontal reference, back-rotation of the 65°E dip angle of the chert and underlying Panorama Fm results in a reconstructed vergence of the fault array towards SSW (Fig. 4A). The basal detachment lies 2550 m below the top of the fault array. Its length amounts to at least 15 km. In analogy with the Kittys Gap and other VSC's (for instance in De Vries et al. 2010), we interpret the sequence of mainly felsic volcanoclastic sediments with minor flows of basalt (basaltic andesite) and intercalations of chert, capped by the stromatolite-bearing SP Chert, deposited close to water level (e.g. Grey et al. 2012).

The chert vein system ascending into the SP Chert, is a feature shared with almost all other VSC's we have analyzed and is indicative of hydrothermal emanation at about zero-water depth during the final stage of VSC formation (Nijman et al. 1998/99a,b; Van Kranendonk 2006; De Vries et al. 2010) which we consider as the aftermath of the volcanic phase of a VSC.

The North Kelly-VSC is atypical because of the near-absence of basalt, in this case the Apex Fm, as basal stratigraphic component above the sole detachment. This becomes relevant in comparison with the Shark Gully-VSC in the Coongan Belt, to be discussed later (Section 3.1).

3. Volcano-sedimentary complexes in the Coongan greenstone belt

The stratigraphic sequence of the Coongan Belt comprises a much wider range of formations than that of the Kelly Belt. It is composed of almost the entire Warrawoona Group, unconformably covered by BIF of the Cleaverville Fm of the basal De Grey Supergroup (Fig. 3A,B). In the Mt. Ada Basalt /Duffer Fm of the Coongan Subgroup, Zegers (1996) and Zegers et al. (1996) recognized a D1 listric growth fault array. These authors related it to the coeval Split Rock Shear Zone in the underlying North Shaw granitoid complex, and interpreted the combination to have developed as an extensional metamorphic core complex; a phase of deformation followed by D2 thrusts causing partial repetition of the stratigraphic column of the belt.

The new satellite imagery interpretations here presented are

[2] [Number] refers, abbreviated, to the MGA grid used in the GSWA 1:100000 geologic map sheets, here applied in Figs. 2, 3, 7 and 8. The first number denotes the longitude, the second the latitude.

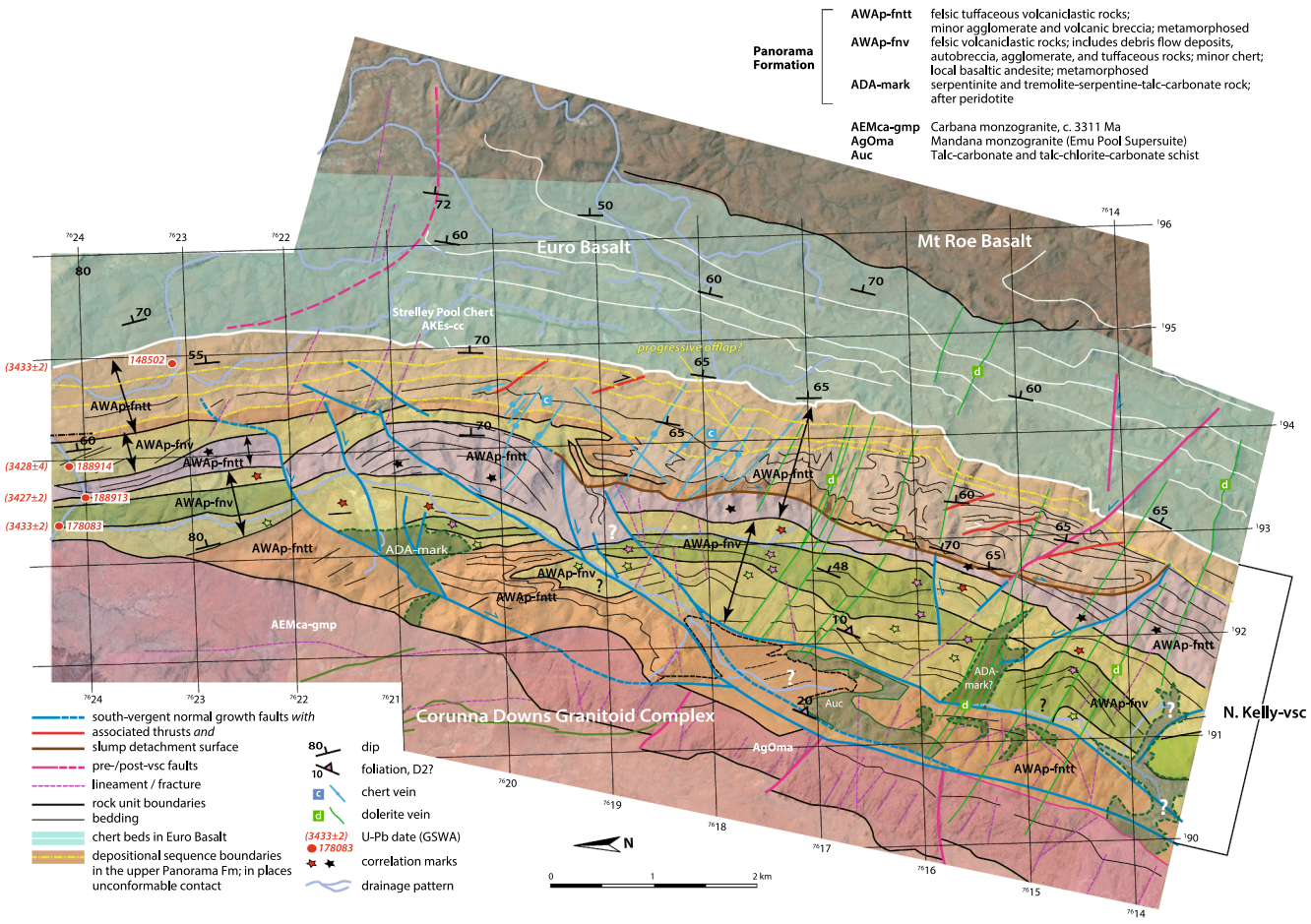

Fig. 2. Geological map of the North Kelly volcano-sedimentary complex, based on new satellite interpretation combined with data from the 1:100 000 geological map sheets Mt Edgar (Williams et al. 2007) and Nullagine (Bagas et al. 2004a) of the Geological Survey of Western Australia. Grid corresponds with the MGA grid used in these maps. Colour differences within the Panorama Fm designate units that can be correlated in satellite image but the individual composition of which is unknown in the absence of sufficient field data. The double arrows refer to the lithological grouping and description of these units according to the legend of the GSWA 1:100 000 maps. (Google Earth: © 2020/2021 CNES/Airbus; Maxar Technologies, recording date 18-7-2018). For the satellite image base, see Supplementary Fig. 2*.

integrated with the latest 1: 100 000 mapping by the GSWA (sheets Marble Bar, Hickman and Van Kranendonk 2008; and Split Rock, Bagas et al. 2003, 2004b) and have resulted in a new interpretation of the D1 deformation. Two superposed VSC's are now distinguished: the *Shark Gully* and *Witnell-VSC's*, named after underlying shear zones detected by Zegers (1996). To determine the tectonic setting of the Shark Gully-VSC, the orientation with respect to the underlying Shaw granitoid complex is of prime importance.

3.1. The Shark Gully volcano-sedimentary complex

Stratigraphy. Above the basal shear zone (Shark Gully Shear Zone: Fig. 3), the Mt Ada Fm consists of basalts with a single komatiite layer and several intercalations of felsic volcanic rock heralding the overlying felsic to intermediate volcanic and volcanoclastic rocks of the Duffer Fm. In satellite images, both formations are well bedded (Fig. 3B), allowing for relatively detailed structural analysis.

The Shark Gully-VSC is separated from the overlying Panorama Fm by one, and in places a set of two subsequent unconformities, and from the Euro Basalt by a roughly stratification-parallel fault. Direct superposition of the felsic units of Duffer and Panorama Fms, with Apex Basalt missing, is confirmed by crystallization ages of 3467 ± 5 Ma and 3468 ± 5 Ma for the Duffer Fm, and 3430 ± 4 Ma for the Panorama Fm, indicating a hiatus of 37 ± 9 Ma (Fig. 3A). The Panorama Fm here is of the same age as in the North Kelly-VSC. Superposition of the two felsic formations is also reported from the west flank of the Shaw complex by Van Kranendonk (2000)[3].

Structure. Schists are associated with the basal shear zone of the Shark Gully-VSC: chlorite-serpentinite-carbonate schist on the north side of the Cooglecong monzogranite intrusion, komatiitic mafic schist on both sides. Within the shear zone, gold has been concentrated (Hickman and Van Kranendonk 2008). Bedding is overturned with dips between 60° and 85° towards W and WSW. Stratigraphic pinching of the Shark Gully-VSC occurs above and on both sides of the 2850 Ma Cooglegong monzogranite. The westward strike deflection on the left hand side in Fig. 3 (north of gridline $^{76}29$) follows the contours of the Shaw granitoid complex.

Within the Shark Gully-VSC, back tilt of the listric normal fault blocks is visible. The satellite images disclosed an extra structural complication: the contact between the Duffer Fm and the underlying Mt Ada Fm evidently served as a secondary extensional detachment offsetting at least two of the listric faults [$^{7}730^{76}270$]. Southwards [$^{7}732^{76}21$], this detachment seems to die out into a local angular

[3] Hickman (2012) extends this observation also to the Panorama Ridge along the southern periphery of the North Pole Dome, where Nijman et al. (2017) propose tectonic duplication of the felsic Panorama Fm by D2 thrusting.

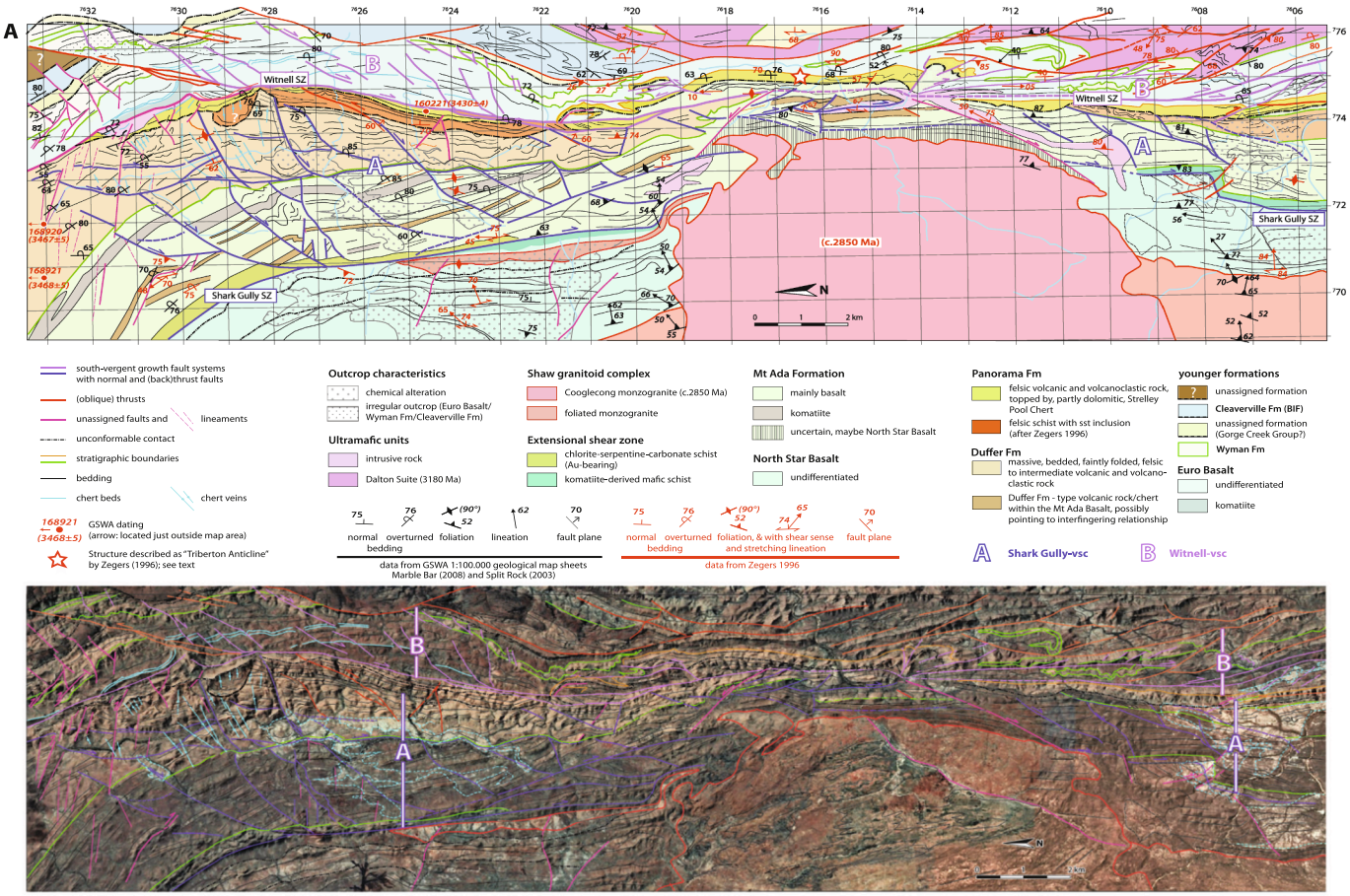

Fig. 3. A. Geological map of the Shark Gully and Witnell volcano-sedimentary complexes in the Coongan greenstone belt, based on new satellite interpretation combined with data from Zegers (1996) and from the 1:100 000 geological map sheets Marble Bar (Hickman and Van Kranendonk 2008) and Split Rock (Bagas et al. 2003) of the Geological Survey of Western Australia. Grid corresponds with the MGA grid used in these maps. B. Satellite image base of Fig. 3A with interpreted stratification and structure pattern. (Google Earth: © 2020/2021 CNES/Airbus, recording date 28-7-2018).

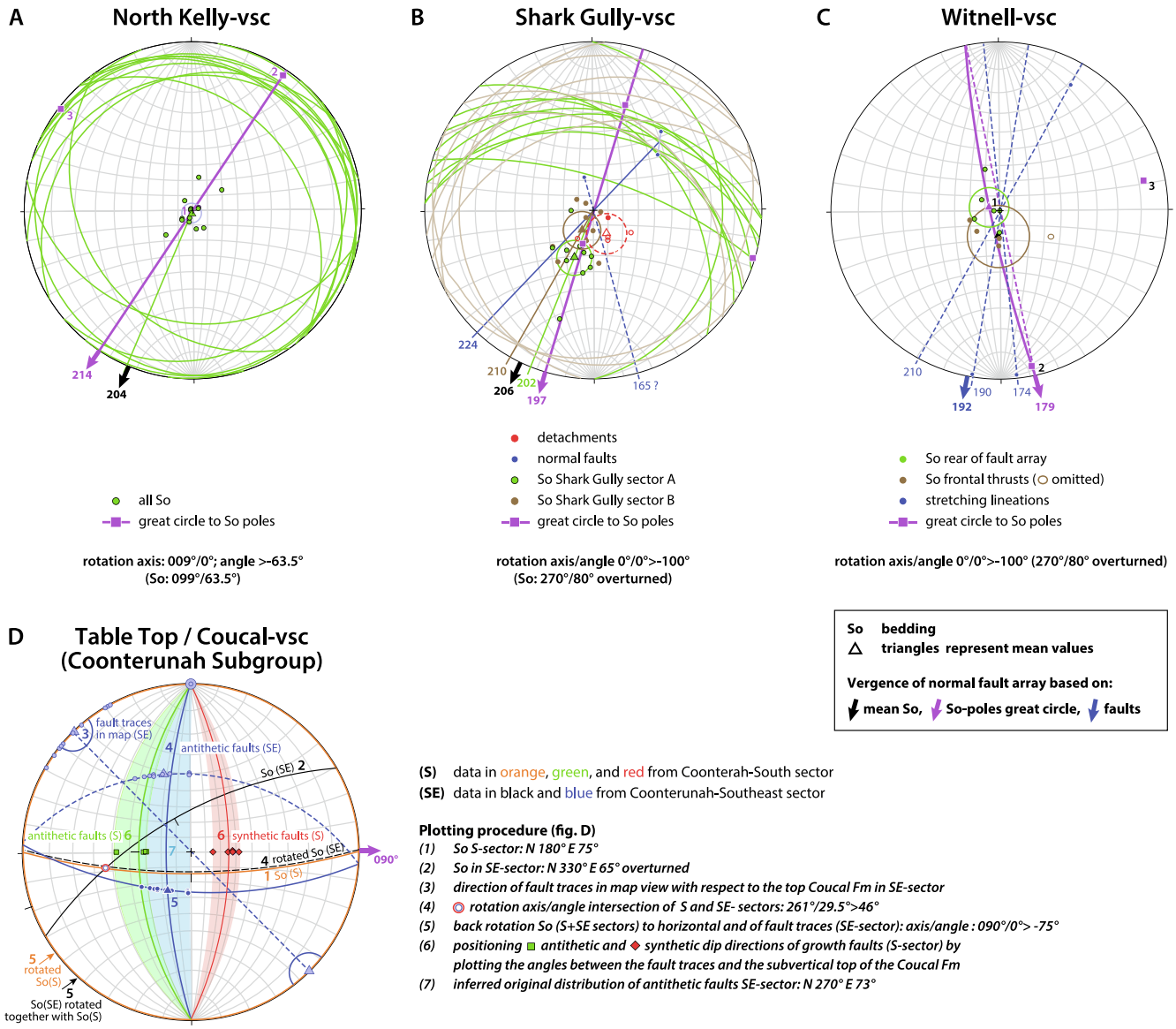

Fig. 4. Equal-angle stereoplots (Allmendinger et al. 2013) of bedding (So), faults and lineations, back-rotated around the strike of the bedding into horizontality of the tops of the newly described VSC's. For the Table Top/Coucal-VSC the complete rotation procedure has been given. Vergence of VSC's derived from mean vectors and from great circle fit of poles on bedding (So), in particular where back-tilted along growth faults, are respectively given in black and violet arrows. Vergence from stretching lineations in the Witnell-VSC is indicated with a blue arrow. Negative rotation angle is anticlockwise. A. North Kelly-VSC (Salgash Subgroup): vergence: N209°E (N204°/214°E). B. Shark Gully-VSC (Coongan Sgr.): vergence N 202°E (N197°/206°E; two normal faults dip N224°E58°). C. Witnell-VSC (Kelly Sgr.): vergence: N186°E (N179°/192°E). D. Table Top/Coucal-VSC (Coonterunah Sgr.): vergence: N90°E.

unconformity.

Back-rotation around the strike of layering at the top of the VSC (currently N270°/80° overturned) to its original horizontal depositional orientation allows determination of.

(1) vergence towards SSW (Fig. 4B);
(2) original detachment depth of 3850 m near the rear of the normal fault array, measured from the Shark Gully detachment towards the unconformity below the Panorama Fm. This is a minimum distance because of unconformable truncation of the top of the VSC. Towards south, the minimum detachment depth decreases to about 2400 m, but this number may have been influenced by later intrusion-related deformation (see below).

The detachment plane bifurcates southwards (Fig. 3A: [$^{7}710^{76}270$]), the upper branch functioning as a low-angle south-verging thrust with vertical foliation. Foliations dipping 63° and 75° ENE along the main detachment north of the Cooglegong intrusion are related to a group of 50°- 85° NE and E dipping foliations measured to the south and north of the intrusion (Fig. 3A). They probably result from D2 compression and do not play a role in the interpretation of the VSC.

Interpretation. Despite a missing stratigraphic top and structural complications, we interpret the Shark Gully-sequence as a VSC with > 60° dipping listric faults. The SSW facing (Fig. 4B) is at an angle with the ENE-WSW extension direction at mid-crustal levels in the 3468 Ma Split Rock Shear Zone (SRSZ) recorded by Zegers (1996) and Zegers et al. (1996). The Shark Gully basal detachment does not visibly connect with the SRSZ in the basement, and extension at upper crustal levels may have been disconnected from lower crustal levels. Hence, the best-fitting scenario at present is one with emphasis on the development of upper-crustal extensional fault arrays that developed in a basin margin prism by gravitational instability resulting in collapse due to lack of lateral support (further discussed in Section 6.2).

3.2. The Witnell volcano-sedimentary complex

Stratigraphy. The stratigraphic sequence above the Shark Gully-VSC consists of 3350–3335 Ma (Hickman 2021) Euro Basalt with intercalated chert beds overlain by felsic volcanic rock of the Wyman Fm (elsewhere in the Pilbara dated at 3325–3315 Ma, Buick et al. 2002). De Grey Supergroup units, amongst which the c. 3020 Ma (Hickman 2021) Cleaverville banded iron formation, lie unconformably on top. On the extreme left (north) in Fig. 3, this sequence is relatively undisturbed, while further southwards faults and folds complicate the picture. Bedding in the Euro Basalt is 60°-80°W overturned, a position similar to that of the Shark Gully-VSC. A thin Wyman Fm rock unit [$^{7}750^{76}235$] seems to be enclosed by basalt, suggesting an interfingering relationship with the Euro Basalt similar to that of the Duffer and Mt Ada Fms in the Shark Gully-VSC and in the basins north of the Warrawoona Lineament (Nijman et al. 2017).

Structure. The rock sequence is fault-bounded over almost the full 26 km length of Fig. 3A. From north to south, the unit shows the following intraformational deformation styles:

(1) a bounding listric normal fault merging into a bedding-parallel shear zone mainly situated along the top of the SP Chert (undistinguished top of the Panorama Fm in Fig. 3), described as the Witnell Shear Zone by Zegers (1996); it shows north-over-south (dextral on the present-day map) shear in (sub)vertical mylonitic foliation;
(2) an array of intraformational, originally south-facing, normal faults [$^{7}755^{76}290$] like those in the underlying Shark Gully-VSC, changing southwards into thrusts and thrust-related folds [$^{7}750^{76}070$];
(3) a sliver of the underlying Panorama Fm and SP Chert right above the Cooglegong intrusion (Triberton Anticline of Zegers 1996, [$^{7}750^{76}170$]; see Interpretation below). The structure shows a symmetric pattern of folds, north-facing on the north side (antithetic with respect to the normal faults), south-facing (synthetic) on the south side; associated stretching lineations plunge 10° to 000° [$^{7}748^{76}185$], 27° to 344° [$^{7}750^{76}204$], and 5° to 183° [$^{7}748^{76}120$].

Interpretation. The interpretation of the structurally disturbed stratigraphic interval of Euro Basalt and Wyman Fm as *Witnell-VSC* (named after the underlying Witnell Shear Zone) should be considered preliminary for reasons given below. The basaltic to felsic Witnell rock sequence is similar to that of the Shark Gully-VSC, as is the S-vergence of syndepositional extensional faults. The length axis of the VSC is derived from the elongate cluster of poles to bedding along a N348°-172°E great circle in the stereonet of Fig. 4C. After back-rotation, the few available stretching lineations plunge at very low angles (2° to 9°) within ± 18° around N192°, in line with the south vergence of the fault array.

Both north and south-verging folds and thrusts of the Triberton structure belong to the VSC. Part of which may be inverted normal faults, where extension changes into contraction. Zegers (1996) interpreted the Triberton structure as a horizontal cross-section parallel to the axis of an east-over-west thrust fold that duplicated Duffer felsic rock. Bagas et al. (2003), however, identified the felsic rock in the Triberton structure as Panorama Fm, supporting its interpretation as part of the Witnell-VSC. More detailed structural field analysis, in particular with respect to kinematic parameters, is necessary to identify the Triberton structure as D1 extension-related.

3.3. Comparison of the *VSC*'s of the Coongan and Kelly belts

In the North Kelly-VSC, 45 km due east of the Coongan Belt, the rock sequence leaves the question unanswered whether the Apex Fm was originally present or absent. In the Coongan Belt, the unconformable superposition of Panorama Fm on Duffer Fm and therefore the absence of the Apex Fm can be explained by time-transgression of the unconformity and onlap of the Panorama Fm over the Duffer Fm, something to be expected in the very margin of a depositional basin (yellow circles in Fig. 5).

The persistence of D1 vergence over a long period, in the Shark Gully, North Kelly and Witnell-VSC's directed southwards, is also common in the superposed basins north of the Warrawoona Lineament. It is particularly well illustrated in the west-facing basin margin of the Coppin Gap Sector of the Marble Bar Belt (Nijman et al. 2017; see also Section 6.3).

On both sides of the Warrawoona Lineament, the vergences are almost 180° opposite (Fig. 5) indicating basin separation along that

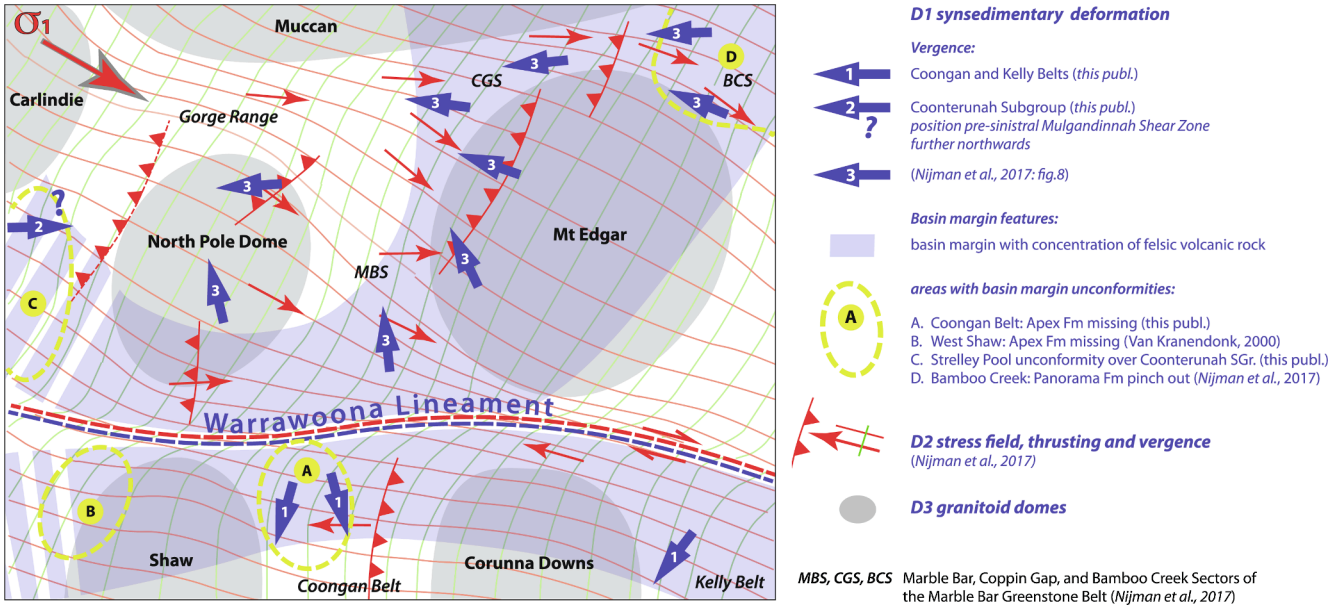

Fig. 5. Schematic presentation of D1 basin features and subsequent structural regimes D2 and D3 in the east Pilbara. Vergence of the D1 normal-faulted volcano-sedimentary complexes (blue arrows) and inferred position of basin margins (blue shade); yellow circles, where important basin margin unconformities have been observed. The background in blurry red shows the subsequent D2 compressive stress field and, as grey ovals, the distribution of D3 granitoid domes (extended after Nijman et al. 2017).

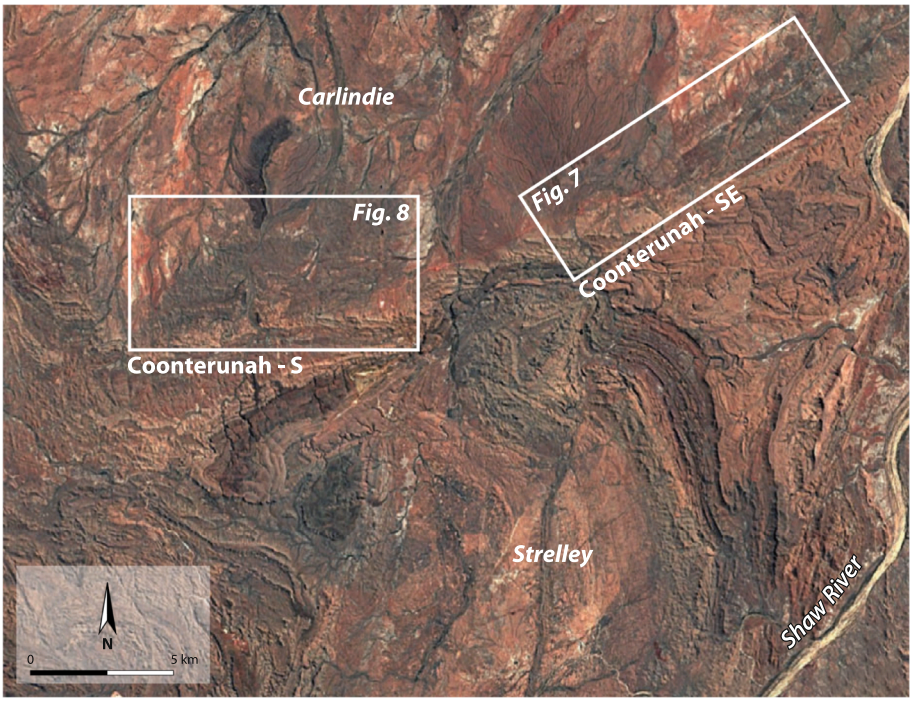

Fig. 6. Satellite image west of the Shaw River, with the position of SE- and S-sectors of the Coonterunah Subgroup shown in maps of Figs. 7 and 8. (Google Earth, Landsat/Copernicus, recording date 31-12-2014).

lineament. It therefore functioned as an important crustal structure *during* the deposition and simultaneous D1 deformation of the Warrawoona Group.

4. The Coonterunah Subgroup: Extension and mega-scale sliding in the oldest part of the Pilbara

In this chapter we present a new interpretation of the Coonterunah Subgroup predominantly based on satellite imagery in combination with already published data. Special attention will be given to the multistorey architecture of the subgroup, including the presence of a volcano-sedimentary complex and of a chaotic unit, interpreted as a mega-scale slide.

4.1. The Coonterunah Subgroup and its multistorey architecture

Stratigraphy. In 1995, Buick et al. identified a rock sequence girdling the south flank of the Carlindie granitoid complex (Fig. 6) as the oldest greenstones of the Pilbara on the basis of a $^{207}Pb/^{206}Pb$ age of 3515.2 ± 2.7 Ma of an interval of felsic rock and chert within mainly tholeiitic basalt (Fig. 7: [$^{7}272^{76}676$]). The sequence was named the Coonterunah Group. It has been intruded by 3467 ± 3.7 Ma old microgranite (geochronology also from Buick et al. 1995) and is separated from the overlying 3426–3350 Ma old SP Chert (Lowe 1983; Hickman 2008, 2021; Wacey et al. 2010) by an angular unconformity. Until then, such an angular unconformity was unknown within the Warrawoona Group.

Van Kranendonk and Morant (1998) subdivided the Coonterunah Group into three formations, the *Table Top Formation* composed of tholeiitic basalt and gabbro, the *Coucal Fm* consisting of a mixture of basalt, andesite, dacite and rhyolite, with black-and white banded cherts along the base and top, and the *Double Bar Fm* consisting of predominantly tholeiitic basalt. Green et al. (2000) and Smithies et al. (2007) further investigated the Coonterunah Group petrologically and geochemically. Since 2006, the Coonterunah Group is considered a subgroup within the Warrawoona Group (Van Kranendonk et al. 2006; Hickman 2011), time equivalent to the Talga Talga Subgroup (Hickman 2021).

Buick et al.'s original time constraint of 3515 ± 3 Ma stems from a sample locality within the lower part of the Coucal Fm (Fig. 7) about 600 m above the base of the formation. Samples from subsequent mapping of Coonterunah outcrops along the east side of the Carlindie granitoid complex (Van Kranendonk et al. 2012) provided three more ages (Nelson 2002): 3498 ± 2 Ma (sample 168995) of rhyolite of the Coucal Fm, and two crystallization ages of 3508 ± 3 Ma (sample 168993) and 3496 ± 4 Ma (sample 168991) from probably Coucal Fm-derived felsic clasts in overlying sediments (additional age information from detrital zircons in Hickman 2021). Hence, the minimum age of the top of the Coucal Fm is c. 3500 Ma, in close correspondence with Hickman's dating of 3498 Ma.

Structure. We analyzed satellite images of the Coonterunah Subgroup in two sectors (Fig. 6), Coonterunah-SE and Coonterunah-S (below also indicated as SE-sector and S-sector), about 5 km strike length separated from each other by a tongue of the Carlindie granitoid complex extending towards the SP Chert Unconformity (Figs. 7 and 8, and Supplementary Fig. 7*, 8*). For the full description of the architecture, as far as distinguishable from satellite images, we refer to the extended captions of Figs. 7 and 8. In both sectors, stratification patterns and structures such as intraformational fault and folds were identified, adding substantially to the existing smaller-scale maps.

A multistorey architecture is evident, consisting of:

(1) An intraformational fault array composed of the upper 2 km (decreasing eastwards to c. 0.5 km) of the Table Top Fm and the c. 1 km (increasing eastwards to 2 km) thick overlying Coucal Fm; the base of the array is only visible in the S-sector of Fig. 8, where it consists of a bedding-parallel fault. Like in the examples described and discussed elsewhere in this study, the stratigraphic sequence affected by this fault array consists of a rock sequence of basalt overlain by a sequence of basalt, felsic volcanic rock and volcanoclastic sandstone and cherts. The very top of the normal-faulted sequence consists of prominent chert beds that only in one

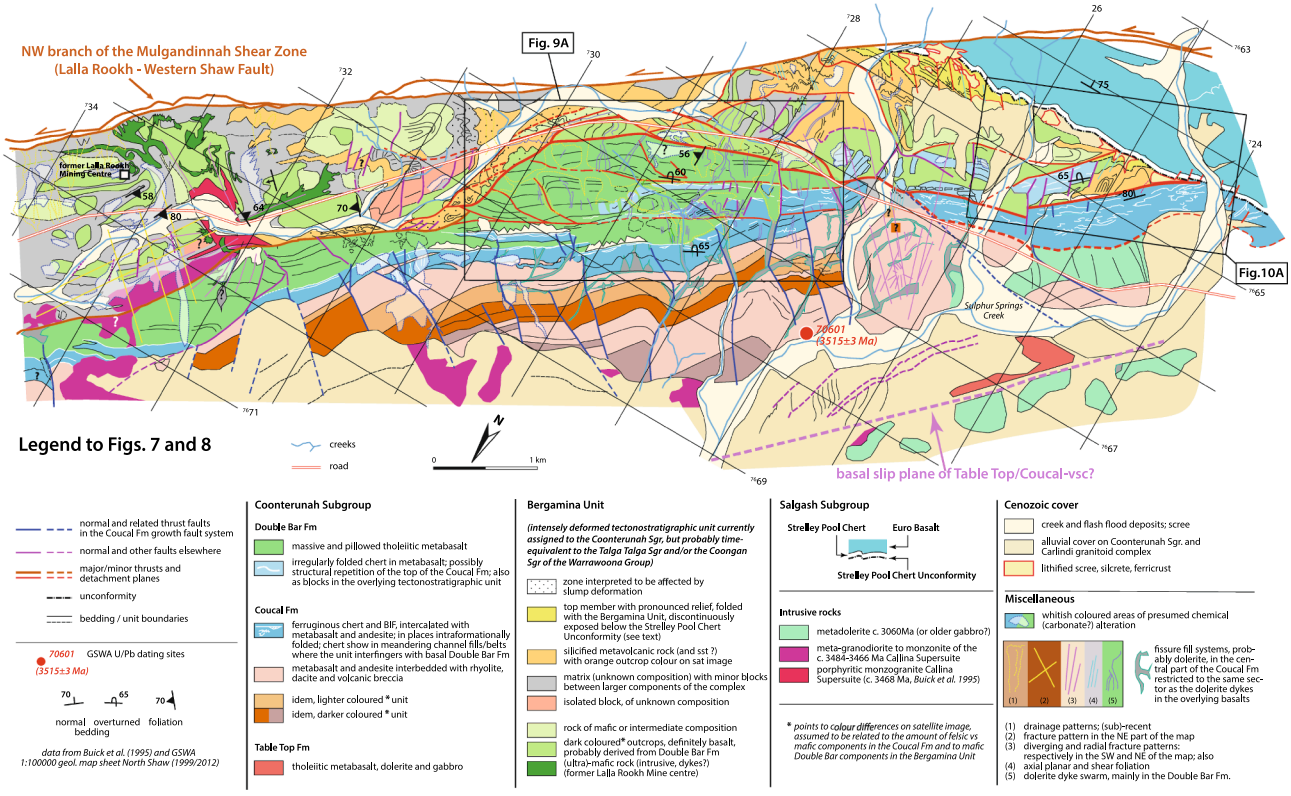

Fig. 7. Geological map of the SE-sector of the Coonterunah Subgroup based on satellite images, combined with data of Buick et al. (1995), Green et al. (2000) and the GSWA 1: 100,000 geological map sheet North Shaw (1st ed. Van Kranendonk 1999; 2nd ed. Hickman 2012). Grid corresponds with the MGA grid used in these maps. Detailed description in accompanying text block. For the satellite image base, see Supplementary Fig. 7*.

Coonterunah SE-sector *(Fig. 7, satellite image in Supplementary Fig. 7*)*. The few published measurements indicate a (sub)vertical dip of the stratification between 65° NW (overturned) and 80° SE (Buick et al. 1995; Van Kranendonk 2000; Hickman 2012). The c. 3.5 Ga Coonterunah Subgroup is truncated obliquely by the 65°-75° S dipping SP Chert unconformity (right hand side of Fig. 7) overlain by the Salgash Subgroup. In turn, the *Lalla Rookh-Western Shaw Fault* (Van Kranendonk 2000) cuts off this sequence, separating it from the much younger De Grey Supergroup sandstone (to the southeast, not indicated in the figure). The fault is the west branch of the *Shaw Structural Corridor* (Hickman 2021), also known as the *Mulgandinnah Shear Zone* (Fig. 1), a major sinistral transcurrent fault zone through the Pilbara craton with a main phase of activity at c. 2950 Ma (Zegers et al. 1998; Van Kranendonk 2008). Largely covered by alluvium, the Carlindie granitoid complex occupies the area in the lower part of the figure. The Coonterunah Subgroup in the SE-sector is c. 3 km thick.

Prominent feature is a *multistorey architecture* of: (1) syn-depositional normal-faulted Coucal Fm with a well-developed chert on top; (2) in the centre of the figure, overlain by stratified basalt of the Double Bar Fm with a few chert-bearing intervals intercalated near its base, and with restricted repetition of beds via several low-angle faults (details in Fig. 9A); and the first two truncated by (3) an undulating low-angle contact below a tectono-stratigraphic unit, here named *Bergamina Unit*, intensely deformed by low-angle thrusts, folds at different scales, and megabrecciation (further description below, next page). Until now, in literature and maps, the Bergamina Unit has been included in the Double Bar Fm, but it consists of a mixture of lithologic components that need further identification in the field. (4) Between the Bergamina Unit and the unconformably overlying SP Chert and partly obscured by crusts of scree or silcrete (see also Wacey et al. 2010), a probably silica (chert?)-rich or silicified top member (GSWA 1: 100000 North Shaw map sheet, 2nd ed., Hickman 2012) appears to be folded together with the underlying Bergamina rocks ([$^{7}270^{76}644$]. The outcrop can be traced into the S-sector (see below).

The GSWA 1: 100 000 map (Van Kranendonk 1999, 2000; Hickman 2012) shows several generations of intrusion. In the left (northeastern) half of figure 7, and arising from the Carlindie granitoid complex, metamonzogranite and -granodiorite of the 3484-3468 Ma Callina Supersuite (Nelson 1999, Van Kranendonk 1999, 2000) intrude into the multistorey architecture. Circa 3065 Ma (Hickman 2012) metadolerite dykes occur in the central part of the map (Figs. 7, 9A) where they swarm upwards from a, probably also dolerite-filled, fissure-system in the Coucal Fm through the Double Bar basalt. In the lower right corner of figure 7, foliated metagabbro (Buick et al. 1995; Hickman 2012) is hosted in the Coucal Fm and in several isolated outcrops in the alluvial plain south of an isolated outcrop of basalt assigned to the Table Top Fm [$^{7}248^{76}645$], the oldest formation of the subgroup. In the GSWA 1:100 000 maps, a major fault has been projected in subcrop between the Table Top basalt and the gabbro. ***(text block continues on the next page)***

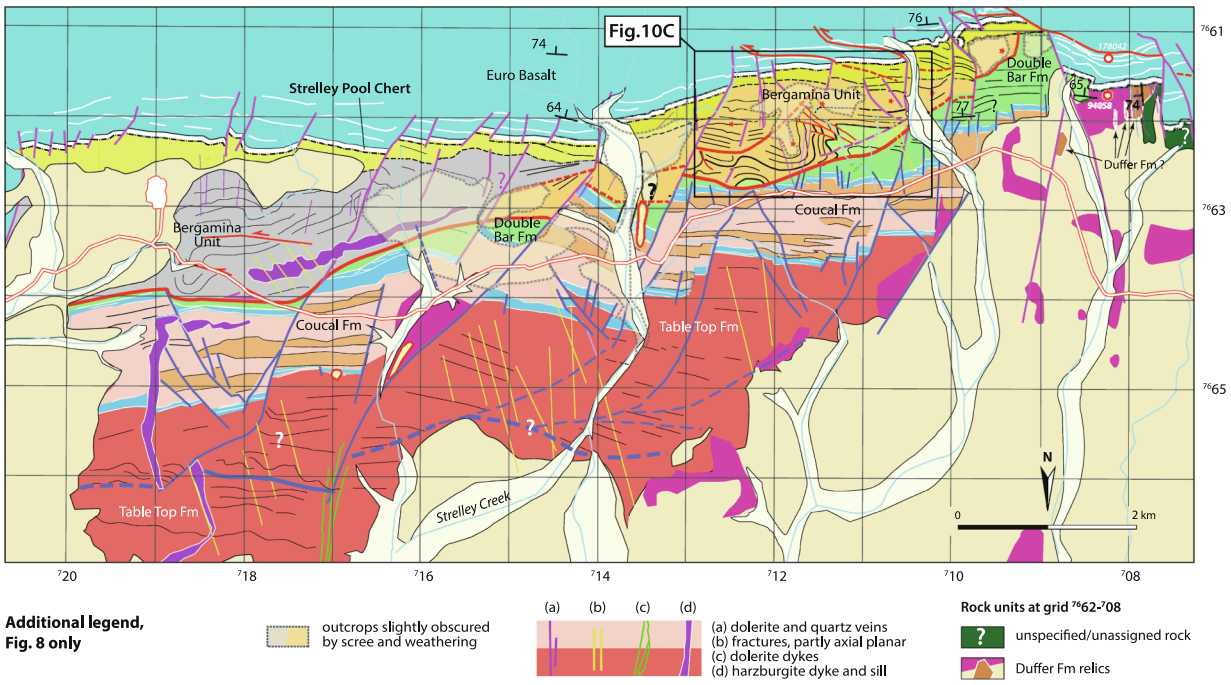

Fig. 8. Geological map of the S-sector of the c. 3.50 Ga Coonterunah Subgroup based on satellite imagery, combined with data of Buick et al. (1995), Green et al. (2000) and GSWA 1: 100,000 geological map sheet North Shaw (1st ed. Van Kranendonk 1999; 2nd ed. Hickman 2012). Grid corresponds with the MGA grid used in these maps. Detailed description in accompanying text block. For the satellite image base, see Supplementary Fig. 8*.

(continued from previous page)

Coonterunah S-sector *(Fig. 8; satellite image: Supplementary Fig. 8*).* The multistorey architecture of the Coonterunah Subgroup is also evident in the S-sector. With subvertical dip (Green et al.2000; 77°S in GSWA map, Hickman 2012), and including an important part of the Table Top Fm, the thickness amounts to 5.9 km. The Coucal Fm contains a second concentration of chert beds along its base, which may also have been present in the SE sector where the lower contact of the formation is not exposed. Most of the Double Bar Fm has been cut out by the low-angle tectonic contact below the overlying Bergamina Unit. The contact climbs westwards in the stratigraphic column, preserving 450 m of Double Bar basalt in the utmost west (right side of figure 8). In the S-sector, too, the scree-covered top member mentioned above sub (2), seems to be present along the top of the Bergamina Unit immediately below the SP Chert Unconformity.

Outside the Bergamina Unit, the dominant deformation visible in the S-sector is east block-down normal faulting, in places with minor antithetic fault effects. Some normal faults terminate within the Coucal Fm, others are truncated by the Bergamina Unit, and some of the larger ones pass through the entire rock sequence.

On the far right side of figure 8 [$^{7}083^{76}616$], Carlindie granite reaches the SP Chert Unconformity. The latter truncates a monzogranite/qtz-fsp porphyry of the Callina Supersuite dated by Buick et al. (1995) at 3467 Ma (geochron 94058), which encases N-S striking slivers of felsic agglomerate, green fuchsite-bearing spherulitic to tuffaceous felsic volcanoclastic rocks, sandstone, and polymictic cobble conglomerate (Van Kranendonk 1999; Hickman et al. 2012) of possible Duffer Fm affinity.

The Bergamina Unit *(The unit is described in four segments from west (Fig. 8) to east (Fig.7))*

(1) In the upper right corner of Fig. 8 ([$^{7}092^{76}610$],details in Fig. 10C), the truncating Bergamina detachment descends from under the SP Chert Unconformity curving eastwards into a low-angle position just above and parallel to the top of the Coucal Fm. Over a distance of 5 km, the dominant rock type is coloured light-brown to orange in satellite image, elsewhere in field-checked outcrops of the east Pilbara a characteristic for felsic or intermediate volcanic and volcanoclastic rocks. The rocks show east-verging inclined folds truncated [$^{7}122^{76}623$] by a secondary detachment plane.

(2) Over the next 5 km eastwards, open-folded and detachment- parallel beds with a few internal low-angle thrusts and normal faults are the main structural features.

Bridging the granite-filled gap between the S- and SE-sectors (see Fig. 5), the Bergamina detachment re-appears from underneath the SP Chert Unconformity. At Sulphur Springs Creek crossing (SE-sector, Fig. 7 [$^{7}240^{76}645$]), it reaches its stratigraphically deepest point.

(3) Over the next 6 km east-northeastwards (Fig. 7), the Bergamina detachment climbs to a culmination, 1 km above the base of the Double Bar Fm [$^{7}292^{76}666$]. The first 3.5 km the unit includes the only here intensely and internally deformed cherty top of the Coucal Fm. The cherts are isoclinally folded with axial planes parallel to the overall stratification, suggesting that the top member of the formation has been stripped from its substratum and sandwiched between two branches of the detachment (details in Fig. 10A,B), while being internally deformed by west-over-east shear. Over the next 2.5 km, the detachment climbs towards its culmination (detail in Fig. 9A).

The lower half of the Bergamina Unit above the detachment consists of mafic rocks, because of their colour in satellite image identified as basalt, and of blocks with rotated bedding similar to the top stratum with deformed chert beds of the Coucal Fm. The upper half of the segment is composed of rock with felsic appearance like the ones mentioned in the SE-sector sub (2). The rocks are deformed by secondary low-angle thrusts, some west-facing thrust folds and an east-facing minor normal fault array ([$^{7}253^{76}650$], Fig. 10A), and upright to east-inclined folds in the upper half of the unit [$^{7}275^{76}650$].

(4) Within 1 km from the culmination northeastwards, the Bergamina detachment descends to 250 m above the top of the Coucal Fm[$^{7}305^{76}686$]. Along the oblique truncation, and where the detachment becomes subparallel to the bedding of the Double Bar Fm, rocks appear to be folded in recumbent to overturned cascade folds (Fig. 9A). Further to the lower left in figure 7, the detachment plane follows a dogleg curve parallel to a flexure in the underlying Coucal Fm, in the foot wall accompanied by an east-over-west low-angle normal fault in the Double Bar/ Coucal Fms. The fabric of the more than 5.5 km long and c. 1.7 km thick segment of Bergamina Unit above the detachment displays a mixture of rock compositions as well as a range of deformations from recumbent and upright folds to normal and thrust faults. One major recumbent fold affects the entire Bergamina Unit at the former Lalla Rookh mining centre [$^{7}334^{76}696$]. Covers of scree and alluvial deposits render lithologic identification difficult, except for the dark-coloured mafic rocks.

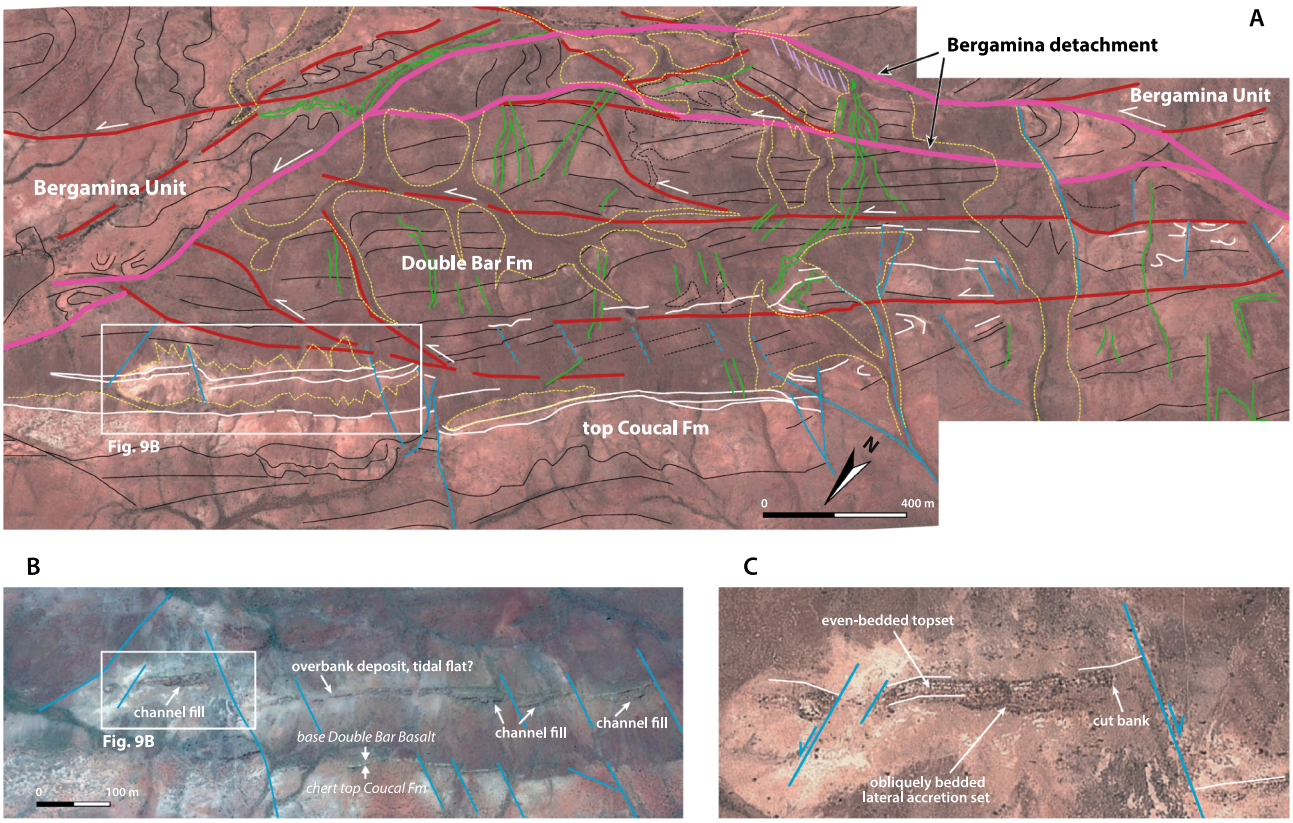

Fig. 9. Satellite image details of the top of the Coucal Fm and of the overlying Double Bar Fm in the centre of the Coonterunah SE-sector (see Fig. 7). A. Superposition of Double Bar basalt upon the chert-bearing top of the Coucal Fm (normal faults in blue, prominent chert beds in white). The Double Bar Fm is dissected by bedding-subparallel faults (red), interpreted to be thrusts related to the emplacement of the overlying Bergamina Unit; violet line is the Bergamina detachment (N.B. the recumbent fault within the detachment zone on the right hand side). The yellow broken lines delineate scree rimming chert outcrops and superficial drainage patterns, for instance caused by sheet flooding. Green lines represent vein systems, probably doleritic (Google Earth: © 2020/2021 Maxar Technologies, recording date 26–8-2011). B. Detail of Fig. 9A: Transition from chert-bearing top of Coucal Fm to Double Bar basalt with enclosed chert unit showing laterally-linked channel fills characteristic of a fluvial or tidal meander belt. (Google Earth: © 2020/2021 CNES/Airbus, recording date 23-11-2015). C. Detail of Fig. 9B with well visible channel fill features like cutbank and lateral accretion (=epsilon) bedding overlain by an even-bedded set, diagnostic for a meandering current system, probably under tidal influence. (Google Earth: © 2020/2021 Maxar Technologies, recording date 26-8-2011).

place, near Sulphur Springs Creek, are intensely folded with axial planes parallel to the stratification.

(2) Regularly-bedded basalts of the Double Bar Fm overlie this faulted stratigraphic complex, but an eastward stratigraphically descending truncation surface, extending over both Coonterunah sectors, leaves only three outcrops of this formation preserved.

(3) Above the truncation, a huge mix of up to one kilometre large fragments of the underlying stratigraphic column and in satellite image unidentifiable or inferred felsic and (ultra)mafic components forms the upper storey of the architecture.

Dykes. The entire Coonterunah Subgroup is traversed by a few late (3070–3060 Ma) dolerite dykes and a single harzburgite dyke (Van Kranendonk 2000; Hickman 2012). The latter ascended through the Table Top and Coucal Fms (Fig. 8) to curve into a sill just below the top cherts of the latter formation. An isolated outcrop [^{7}170^{75}635] is situated within the unit above the truncation surface and roughly parallel to it. It is not clear whether the harzburgite intrusion is of *syn*-Coucal or later age. If its age were *syn*-Coucal, the harzburgite enveloped in the overlying chaotic unit would be allochthonous.

Interpretation. We interpret the major listric normal faults with downwards increasing offset and back tilt below the stratigraphic level of the Double Bar Fm in the S-sector as east-facing, leading, synthetic growth faults. The set of minor straight, northwest-striking normal faults in the Coucal Fm of the SE-sector, and a series of minor faults in the S-sector, are interpreted to be antithetic (see also Section 4.4). Towards deeper levels, the synthetic normal faults merge with what appears to be a bedding-parallel detachment, at a maximum just over 2 km below the top of the Table Top Fm in the S-Sector. Although the satellite images of the Table Top Fm are not very decisive in localizing this detachment, the sequence from basaltic Table Top Fm towards a black-and-white chert-bearing assemblage of basalt, andesite, dacite and rhyolite of the Coucal Fm, combined with the listric growth-fault style deformation are features characterizing VSC's also elsewhere in the Pilbara and in the Barberton greenstone belt of South Africa (see Section 5).

In summary, the normal-faulted upper Table Top and Coucal sequence of basalt to felsic volcanic rock and chert can be characterized as a volcano-sedimentary complex, the *Table Top/Coucal-VSC*.

The chaotic unit above the truncation surface is here named the *Bergamina Unit* (*new name* after the Bergamina shaft in the former Lalla Rookh (gold) Mining Centre, Fig. 7). Details of both units are discussed below.

4.2. The Table Top/Coucal volcano-sedimentary complex, details

In addition to the detailed description of the Table Top-Coucal sequence accompanying Figs. 7 and 8, a few more features, useful for the interpretation as a VSC and its comparison with the other examples, are highlighted.

The transition from Coucal Fm to the overlying Double Bar Fm. The transition is gradual because the chert-rich facies in the top of the Coucal Fm recurs in the lower part of the Double Bar basalt (Fig. 7). When

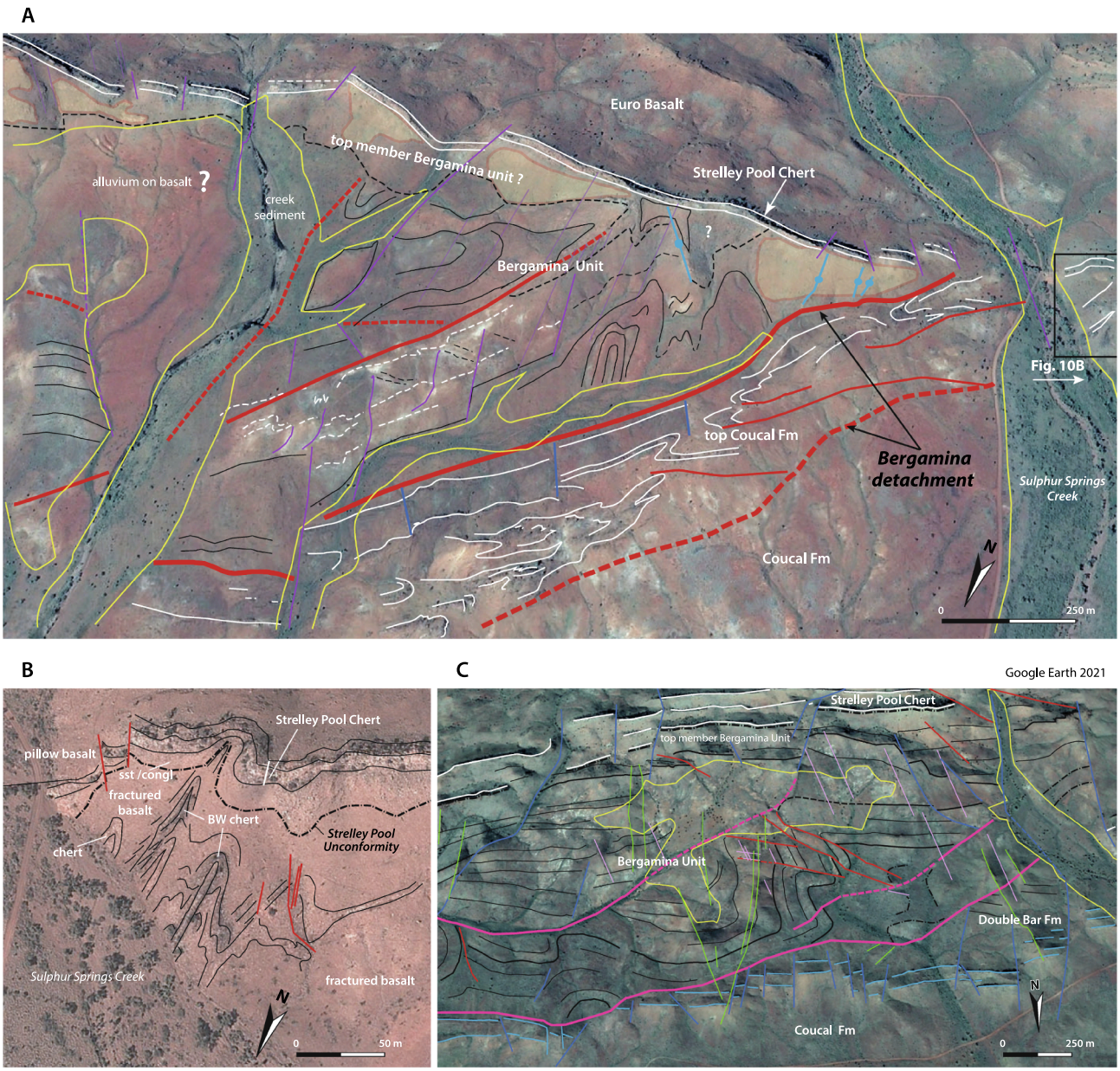

Fig. 10. Satellite image details of the Bergamina tectonostratigraphic Unit. A. Superposition of the folded and faulted Bergamina Unit upon the internally strongly shear-deformed chert-bearing top member of the Coucal Fm, at (Fig. 10B) and immediately east of Sulphur Springs Creek. (Google Earth: © 2020/2021 CNES/Airbus, recording date 13–7-2013). B. Detail of Fig. 10A at Sulphur Springs Creek: paleorelief over isoclinally folded chert/basalt of the Coucal Fm below the angular Strelley Pool Chert Unconformity. (Google Earth: © 2020/2021 Maxar Technologies, recording date 26–8-2011); see also figure16 in Van Kranendonk 2000. C. Detail of east-verging folding above the detachment of the Bergamina Unit in the utmost western part of the Coonterunah-S sector (Fig. 8), where the rear of the detachment plane descends from below the Strelley Pool Chert Unconformity through the Double Bar Fm towards the top of the Coucal Fm. (Google Earth: © 2020/2021 Maxar Technologies, recording date 24–6-2018).

zoomed-in (Fig. 9A > B > C), the satellite images show that the structurally undisturbed chert in the very top of the Coucal Fm represents a system of laterally-linked channel fills. The immediately overlying Double Bar basalt encloses a similar, 1.3 km long, chert layer of laterally-linked channel fills. One of these (Fig. 9C) shows lateral-accretion bedding (oblique bedding with dip direction parallel to the channel cross-section), overlapped by an even-bedded top set, and a preserved cut bank. The accretion bedding is diagnostic for meandering channels in lowland river systems, tidal environments and deeper-water turbidite fans The even-bedded top set is reminiscent of tidal flat deposition.

The similarity of this transition with the one observed in the field along the top of Kittys Gap-VSC (De Vries et al. 2010) is striking. There, the transition is interpreted as a system of laterally-linked tidal flat and channel-fill cherts in the top of the VSC, upwards fading away towards isolated meandering channel fills within the overlying Euro Basalt. Such a sedimentologic setting indicates deposition at about water level, an interpretation here applied to the top of the Coucal Fm and the transition into the Double Bar basalt.

Further westwards in the SE-sector, for instance at Sulphur Springs Creek (Fig. 10A,B), the chert beds in the top of the Coucal Fm are tightly folded and recumbent (see detail in Fig. 10B, field-checked in Van Kranendonk et al. 2001). We interpret this local intense internal deformation in the top member of the Coucal Fm as directly related with displacement and deformation of the Bergamina Unit (see Section 4.3 sub 3).

Based on the similarity with the Kittys Gap-VSC the depositional

environment of the sequence appears to be shallowing-up, which of course demands field truthing. Assuming that the localization of the detachment plane in the S-sector is correct, the crustal depth of the base of the VSC can be determined at 3000 m; in the SE-sector a minimum depth estimate is 2000 m. The exposed length of the normal fault array, added over both sectors, is 22 km.

4.3. The Bergamina tectonostratigraphic Unit

Structure from satellite imagery. In the figure caption of Figs. 7 and 8 the variety of deformation styles in the Bergamina Unit is described for four segments from west (right-hand side of Fig. 8: S-sector) to northeast (left-hand side of Fig. 7: SE-sector). Details of deformation are illustrated in the satellite images of Figs. 9 and 10.

Interpretation of the Bergamina Unit. Four key arguments form the basis of our interpretation of this area. The interpretation has uncertainty because of the lack of field ground-truthing. Hence, our preferred, as well as alternative interpretations, are outlined and discussed.

(1) The Bergamina Unit is intensely deformed. The deformation cannot be caused by the relatively late, sinistral displacement along the Lalla Rookh-Western Shaw Fault because of much earlier truncation of the unit and its structures by the 3426 Ma SP Chert Unconformity (cf Figs. 7 and 8 and accompanying text).
(2) The unit is lithologically diverse, (ultra)mafic and felsic, with isolated, in places rotated blocks, most of them of unknown provenance. Some are recognizably derived from the Coucal Fm, others fault-bounded slices still almost attached to the Double Bar Fm.
(3) The unit is tectonically displaced over a basal low-angle detachment, eastwards descending into the stratigraphy through the Double Bar Fm, undulating with depressions and a culmination. Where in the SE-sector the detachment climbs eastwards stratigraphically against a culmination, low-angle thrusts, back thrusts and stratigraphic repetitions prevail (contraction), while behind the culmination cascade folds suggest free sliding down the truncation plane (local extension). The joint occurrence and distribution of a wide range of local contractional and extensional structures, as well as a mixture of lithologically different blocks, are diagnostic for deformation related to slope failure and slumping. The most obvious interpretation of the forming of the Bergamina Unit is therefore a down-slope gravitational displacement, such as a subaqueous debris avalanche (Masson et al. 2006, see further Sections 4.4. and 6.3). Other mechanisms may have been a major landslide, or a chaotic mass displacement due to a meteorite impact (cf. Byerly et al. 2002; Glikson and Vickers 2010; and in particular because of synchronism with the Duffer Fm: Glikson et al. 2016; see below).
(4) The Bergamina Unit is possibly age-equivalent to the Duffer Fm. It was emplaced between deposition of the uppermost preserved beds of the Double Bar Fm and the intrusion of the Callina Supersuite (3484–3466 Ma, age range in and around the Carlindie Dome according to Hickman 2021). The maximum age corresponds with that of the youngest preserved Double Bar basalt, in the culmination within the SE-sector, stratigraphically c. 950 m above the top of the Coucal Fm (Fig. 7). To estimate the age of the Double Bar basalt in that locality in the absence of sufficient direct age constraints, we take for reference the average vertical accretion rate of 10 km in 40 Ma (250 m/Ma)[4]. The c. 950 m thickness of preserved Double Bar Fm then accounts for c. 4 Ma, which brings the age estimate for the youngest Double Bar basalt at c. 3496 Ma, 4 Ma year younger than the above calculated age of c. 3500 Ma for the top of the Coucal Fm. Unknown, of course, is how deep the Double Bar Fm has been truncated by the Bergamina avalanche. For the top of the formation Hickman (2021) mentions an age of 3490 Ma.

From these age constraints the emplacement of the Bergamina Unit can then be calculated to have taken place within a *minimum* time slot of c. 6 Ma, 3490–3484 Ma, within the range of the Talga Talga Subgroup further eastwards in the Pilbara. Alternatively, the *maximum* time slot amounts to c. 30 Ma (3496–3466 Ma), including the period of deposition of the Duffer Fm (Coongan Subgroup). In this respect, the observation of Duffer Fm rocks as slivers in the 4667 Ma Callina monzogranite at the rear of the Bergamina Unit, mentioned in the extended caption of Figs. 7 and 8, needs further investigation and confirmation.

4.4. Restoration of the Coonterunah cross-section.

The restoration procedure. The equal-scale cross-section of Fig. 11 relies on back rotation of the Coonterunah sequence based on the following observations:

(1) The subparallel position, *i.e.* without angularity, of the Coonterunah Subgroup and the unconformably overlying SP Chert / Euro Basalt in the S-sector (N180°E75°, Fig. 8) is the normal stratigraphic configuration where a hiatus is observed elsewhere in the Pilbara (cf. in the yellow circles in Fig. 5). This position has been used for back-rotation.
(2) The abnormal, overturned N336°E65° position of the Coonterunah-SE sequence was reached before deposition of the SP Chert, possibly linked with post-Bergamina faulting or flexuring related to intrusion of the Carlindie granite. As a consequence, the first step to be made in restoring the cross-section to its original position is to rotate the cross-section of the SE-sector (Fig. 7) back into a position aligned with that of the S-sector (Fig. 8) around their intersection.
(3) The strike deviation of the bedding towards NW in the Table Top Fm, here explained as being caused by back tilt along a bounding fault of the VSC, is used in determining synthetic and antithetic attitude of the normal faults.
(4) The subvertical bedding in the top chert of the Coucal Fm and the base of the Double Bar Fm was originally horizontal and at water level (Fig. 9). The large angle (>60°) the normal faults make in satellite view with the originally horizontal top of the VSC indicates that the cross-section in map view is approximately at right angles to the strike of the faults of the array. It therefore closely corresponds with the original cross-section along the longitudinal axis of the array. Consequently, the acute angle between the faults and the top of the VSC, measured in the map of Fig. 8, can be used to plot the positions of synthetic and antithetic faults.

Even with the few measurements of bedding orientation actually available, the rotation procedure (Fig. 4D) renders due east vergence of the extensional faults of the Table Top/Coucal-VSC in the S-sector evident. The alignment of the SE-sector with the S-sector also implies rotation of the fault traces in outcrop (*i.e.* in the map view of Fig. 7) within the VSC.

For the Bergamina Unit east vergence is in agreement with the upright, inclined, recumbent to overturned fold patterns and minor normal fault arrays. Transport along the basal detachment was therefore west-over-east. The large dip angle of the normal faults in the present outcrop of the Coucal Fm suggests the actual cross-section to be oriented not far from parallel to the vergence, a conclusion for which more field-

[4] The accumulation rate is derived from the basalt-dominated Warrawoona Group in the Central Coppin Gap Sector of the Marble Bar Belt (Fig. 1 for location) (Nijman et al. 2017); cf. in the Barberton Greenstone Belt: 225 m/Ma for the Hooggenoeg Fm with comparable lithological variation (De Wit et al. 2018, *p.652:* 2700 m in 12 Ma [c. 3472–3460 Ma]).

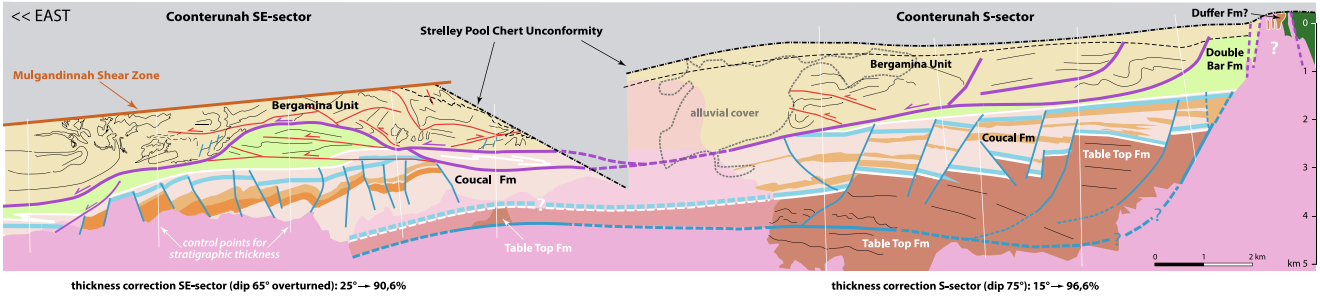

Fig. 11. Reconstruction of the Coonterunah cross-section, by back rotation towards a position preceding both the Strelley Pool Chert Unconformity and the deflection of the Coonterunah SE sector with respect to the S-sector (cf Fig. 4D). No vertical scale exaggeration. The reconstruction illustrates the syn-/antithetic fault array of the Table Top/Coucal volcano-sedimentary complex and the Bergamina Unit above the gradually eastwards-descending detachment plane, with its variety of internal deformations. Note that the Carlindie granitoid complex (pink-coloured), definitely younger than the Coonterunah Subgroup, is depicted only to indicate lost parts of the cross-section and where intrapolated between the S- and SE- sectors.

based structural analysis, such as measurements of bedding, fold axes etc., would provide more control.

Multistorey architecture, an interpretation. The restored cross-section of Fig. 11 illustrates the multistorey architecture of the Coonterunah Subgroup. We propose the following scenario for its origin. The rock sequence from tholeiitic basalt (Table Top Fm), felsic rock with basalt and chert beds (Coucal Fm), and again tholeiitic basalt (Double Bar Fm) is similar to the younger sequence of the North Star Basalt, Dresser Fm and Mt Ada Basalt in the North Pole Dome on the opposite side of the Mulgandinnah Fault Zone. In terms of basin development, our environmental interpretation of such a sequence is subaquatic (probably sub*marine;* often pillowed basalt of unknown depth, see also Section 6.2) shallowing to zero water depth and subsiding again to the pillow-basalt depth (De Vries et al. 2006a, 2010).

The extensional deformation in the shallowing-up Table Top/Coucal-VSC is of the same type as in younger VSC's elsewhere in the Pilbara, consisting of a normal fault array activated during build-up of an unbalanced basin margin prism. It is the only example with synthetic and many antithetic normal faults. The flexure with secondary detachment, observed below the northeastern segment of the main detachment, is interpreted as due to slope collapse concurrent with or immediately prior to sliding of the Bergamina Unit.

If subsequent deepening during deposition of the Double Bar Basalt was considerable, the basin margin evidently became unstable enough to accommodate gravitational emplacement of an avalanche the size of the Bergamina Unit. If so, the unit should be considered a *base-of-slope deposit of an east-facing basin margin* further to the west.

5. The Buck Reef volcano-sedimentary complex, Barberton greenstone belt, South Africa

The South African Paleoarchean Buck Reef (BR)-VSC serves as an, in terms of architecture, very complete standard with which the VSC's of the Pilbara can be compared.

The c. 3.45 Ga old (review of geochronology in De Wit et al. 2011, 2018) rock sequence of the Buck Reef Chert (abbreviated BRC, previously also named Buck *Ridge* Chert) has been described in detail (e.g. Lowe and Byerly 1999, 2020; Lowe et al. 2012; Tice and Lowe 2006; De Vries et al. 2006b, 2010; Furnes et al. 2013; De Wit et al. 2011, 2018; Ledevin et al. 2019). The geological map (Fig. 12A) of the BR-VSC (Nijman and De Vries 2005) is based on extensive 1:10000 field mapping and aerial photo interpretation, complemented by data from Dann (2000) and unpublished maps and field data of De Wit, King, De Ronde, and Smith (for reliability map and references, see Nijman and De Vries 2005). The map is the basis for the reconstruction of the original geometry in Fig. 12B.

5.1. Architecture of the Buck Reef-VSC

Stratigraphy. The >2 km thick VSC is composed of basalt, making way in the younging direction for increasingly thicker intercalations of felsic volcanic rocks, alternating upwards with sedimentary cherts to finally form a locally >600 m thick succession of sedimentary cherts (Fig. 12). The VSC has been intruded by mainly porphyritic TTG (tonalite-trondhjemite-granodiorite), both as massive rock bodies and as sills. These rocks and the associated felsic volcanic and volcanoclastic rocks of the BR-VSC are dated 3451 ± 5 Ma by De Vries et al. (2006b). The age range of the entire BR-VSC is given as 3452–3445 Ma in De Wit et al. (2018), isochronous with the Panorama Fm in the Pilbara. Of the five chert units (BRC-Units 0–4), the oldest one (BRC-Unit 0) is only fully developed at the western toe of the VSC. It tapers out 3.5 km eastwards within the basalt-felsic volcanic suite where it has a considerable back tilt (see section on Structure below). BRC-Unit 1 has an interfingering contact with the underlying felsic rock and together with BRC-Units 2–4 forms the cap of the VSC.

Lowe and Byerly (1999, 2020) consider the mafic and felsic components of the BR-VSC as the uppermost part of the Hooggenoeg Fm (*their unit H6),* and the BRC-Units 1–4 as the unconformably overlying basal unit of the Kromberg Fm (*their unit K1c)*. De Wit et al. (2011, 2018), on the other hand, merged the entire BR-VSC in a newly created Noisy Complex, fully assigned to the basal Kromberg Fm, without intraformational unconformity. In Fig. 12 we follow the latter assignment. The stratigraphic indivisibility of the basalt-felsic volcanic/volcanoclastic rock to chert sequence of the BRC-VSC, expressed by the interfingering relationship of all of its components (Fig. 12), is in the context of this article more relevant than the question concerning what formation the BRC-VSC has to be assigned to.

Structure. The BR-VSC is subdivided by 3 to 4 km-spaced major listric normal faults, a division still visible in the actual drainage pattern and relief (Fig. 12A). These faults controlled the distribution and asymmetrical shape of TTG intrusions. Maximum thickness in the hanging walls, and minimum thickness in the footwalls are associated with up to 60° tilt of the bedding against the major normal fault. In the western half of the cross-section, tilt accompanied by a roll-over anticline caused a local intraformational unconformity below BRC-Units 1 over the anticlinal crest.

The normal faults merge as major listric features with a complex of superposed shear zones along the base of the BR-VSC (Fig. 12B). The majority of folds and minor thrust faults in the immediately underlying Waterfall Chert (see legend to Fig. 12; *unit H5 of* Lowe and Byerly 1999) verge westwards, synthetically with the sense of displacement along the normal faults above and within the basal shear zone. The latter therefore served as a sole detachment to the extension in the normal fault array and separates the deformed BR-VSC from the underlying, less disturbed

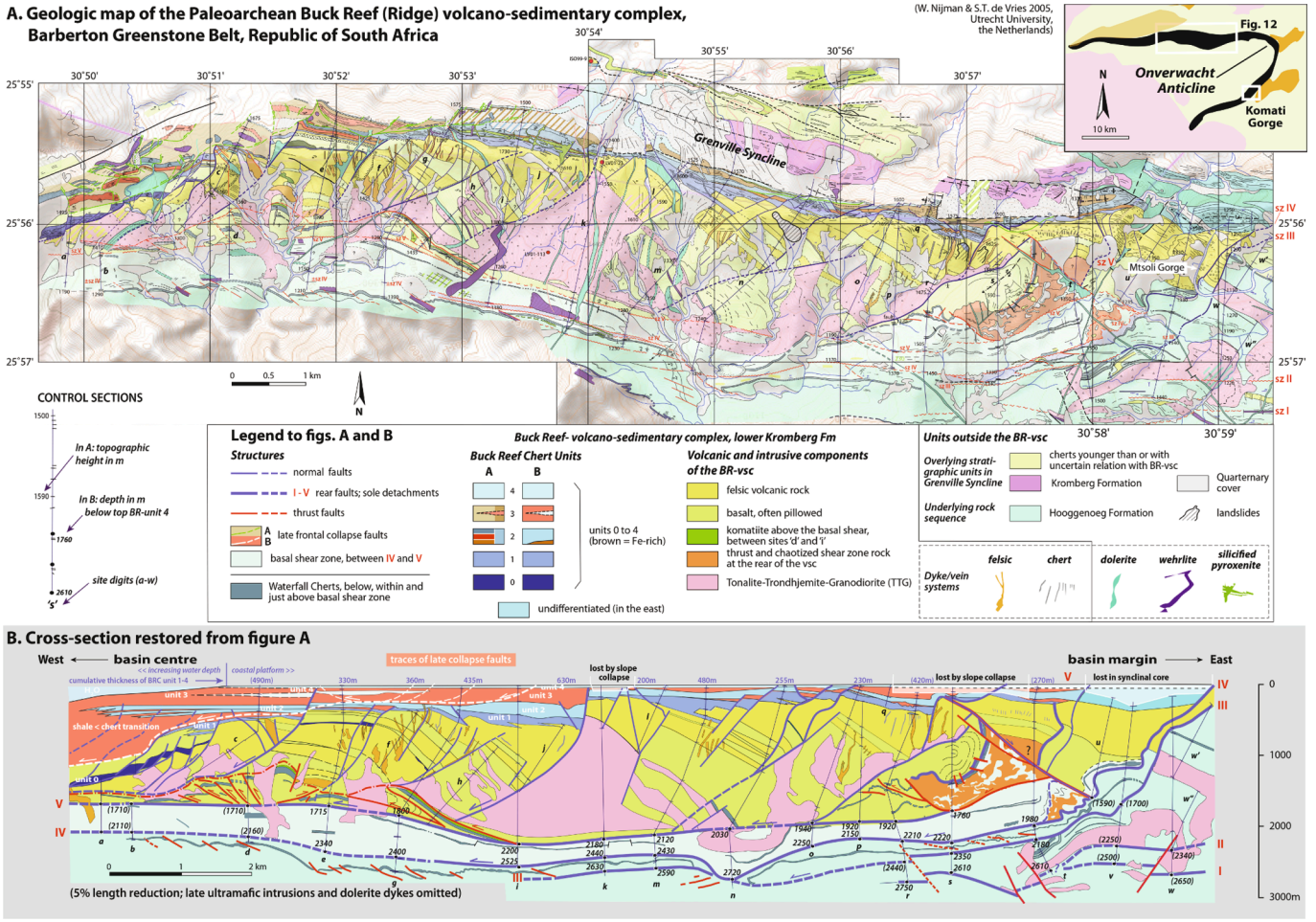

Fig. 12. A. Geological map of the c. 3.45 Ga Buck Reef volcano-sedimentary complex, Barberton greenstone belt, RSA (after Nijman and De Vries 2005), adjusted to an underlying topo graphic contour map, and showing the positions of 23 cross sections ('a' – 'w') used in Fig. 12B. Inset map shows the position of the BRC-VSC in the north limb of the Onverwacht Anticline and the Komati Gorge locality in the southeast limb, discussed in the text. B. Restoration of the Buck Reef-VSC of (A) by suspending stratigraphic columns of the cross-sections 'a' – 'w' from the straightened chert top (BR Chert-unit 4) of the complex.

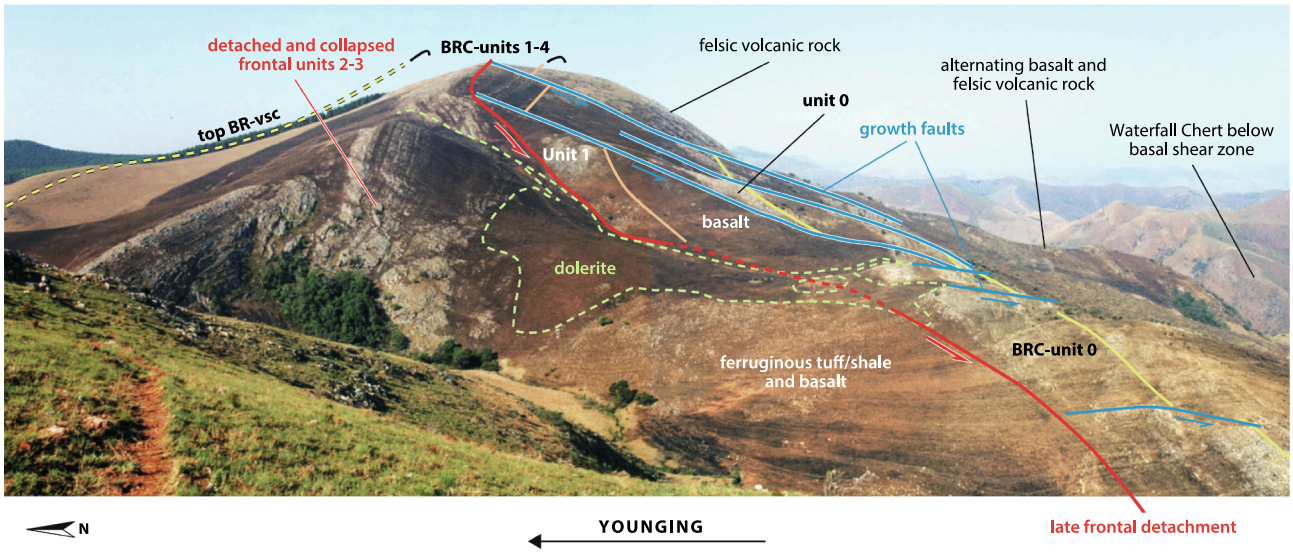

Fig. 13. Gravitational deformation in the basin margin platform slope of the 3.45 Ga Buck Reef-VSC, Barberton greenstone belt. Eastward view across the depositional slope of the complex towards the shallow-water platform of the basin margin cherts, between cross-sections 'a' and 'e' in Fig. 12. Normal growth faults (blue) accommodate stepwise stratigraphic expansion towards the viewer. BR Chert-units 2–4 of the basin margin frontal slope collapsed into blocks, jumbled within ferruginous shale and tuff of the platform slope. Dolerite dykes are younger than the BR-VSC.

mafic rock succession of the Hooggenoeg Fm (Dann, 2000). Just above the shear zone, slabs of chert, probably picked up from the underlying cherts, occur partly in overturned position, partly in piggy-back thrust arrangement.

At the toe of the fault array, in the west (left-hand side in Fig. 12A), BRC-Units 2–4 have been detached from the main body of the BR-VSC, broken up, chaotically juxtaposed, and thrust upon each other within a matrix of Fe-rich shale (Fig. 12A, 13). At the rear of the normal-fault array, in the east, the normal faults are folded, accompanied by an overturned fold and chaotized units derived from the sole detachment.

Dykes and veins. Apart from two post-BR-VSC dyke generations (2967 ± 1 Ma [Olson et al. 2010] dolerite, and c. 3228 Ma pyroxene-amphibole porphyry [De Vries et al. 2006b]), several dyke and vein systems successively cross-cut the BR-VSC reaching to successively higher stratigraphic levels of the BRC (Fig. 12A; relative ages based on field relationships). Consecutively, their composition is felsic and black chert, then fine-grained mafic, and finally ultramafic (wehrlite). The wehrlite dykes end, and spread as sills, in the overlying unit of the Kromberg Formation. This observation is very similar to the one in the Coonterunah S-sector of the Pilbara (Fig. 8) where ultramafic (harzburgite) dykes transect the Table Top/Coucal-VSC to terminate just above the complex as sills.

Interpretation. In previous publications (Nijman and De Vries 2004; De Vries et al. 2006, 2010), we have interpreted the BR-VSC as a growth-fault controlled, partly chaotized, bimodal volcanic complex, with felsic volcanism becoming increasingly dominant upwards. The *syn*-depositional intrusion of felsic (TTG) rock along the major faults was accompanied by felsic dykes, chert veins, and hydrothermal circulation in the top of the complex.

The facies of the BR-VSC changes from conglomerate in the easternmost felsic volcanic part of the VSC(e.g. at Mtsoli River Gorge, Fig. 12A), westwards along the BRC via a coastal platform to a shale-dominated slope with collapse structures (Fig. 13). These rocks overlie and interdigitate with pillow basalts and the sequence as a whole has been interpreted as shoaling upwards with a final transgressive switch from BRC-Unit 2 upwards (Supplementary Fig. 13*). Combined with the normal fault structure, this architecture supports the interpretation of the BR-VSC as westward-facing basin-margin deposystem. The basin is here called the *Mtsoli Basin* (Table 1). A volcanic edifice, supposed to have been situated in the basin centre further westwards, is held responsible for large eastward (coastward)-filled cut-and-fill structures in BRC-Unit 1 (*figure 6 in* De Vries et al. 2010).

The slumping along the slope in the toe of the VSC (Fig. 13) was a late-stage process as it involved only BRC-Units 2–4, and probably also the ultramafic wehrlite intrusions (omitted in Fig. 12B), intruded shortly after deposition of BRC-Unit 4.

The folding of normal faults at the rear side of the VSC is explained by additional gravitational collapse and slip of fault wedges along the main detachment surface within the space created by extension at the rear of a fault array. The progressive deformation of growth faults at the rear points to backstepping of the bounding fault of the growth fault array (Gibbs 1984; McClay and Scott 1991; Imber et al. 2003).

The order of appearance of the dykes and veins (felsic/black chert-mafic–ultramafic) matches the depositional sequence and compositional change in the BR-VSC host rock from felsic volcanic rock to chert in BRC-Unit 1, via Fe-enriched chert and shale of BRC-Unit 3, to overlying (ultra)mafic volcanic rock. The successive dykes and veins are therefore interpreted to be coeval with the building-up of that succession.

5.2. *Restoration of the BR-**VSC** cross-section*

The original architecture of the BR-VSC has been reconstructed by suspending 23 stratigraphic profiles ('a' to 'w' in Fig. 12A and B) from the straightened and horizontalized uppermost BRC-Unit 4. Unit 4 is taken as reference, because at that top level of the VSC the growth-fault offset has decreased to zero. The reconstruction consists of:

- back-rotation to horizontal of the BRC and underlying sequence from its 80° overturned position;
- 5 % length reduction of the cross-section to correct for the obliquity of the outcrop section with respect to a cross-section at right angles to the strike of the normal faults; and.
- restoration of the front of the VSC (on the extreme left hand side of Fig. 12B) by putting the displaced chert slabs (Fig. 13) back into their original position.

The reconstruction (Fig. 12B) shows a 17 km long listric normal fault array with:

Table 1

Basin name	*Formations involved*	*Name of VSC* **	*Age in Ma*	*Exposed length (km)*	*Detachment depth below sea level (m)*	*Minimum inferred, basin floor depth (m)*
Kelly Basin*	Euro Basalt-Wyman	***Witnell***	c. 3315	25	min. 1500	**1500**
South Salgash Basin	Panorama-Strelley Pool; (Apex Fm ?)	***North Kelly***	c.3430	15	2550	**2500**
North Salgash Basin	Apex-Panorama-Strelley Pool	***Panorama North***	c.3440	>8	c.1000	**1000**
	Apex-Panorama-Strelley Pool	***Kittys Gap***	c.3445	c.10	1250	**1200**
	Towers-Apex-Strelley Pool	***Bamboo Creek South***	c.3460 - c.3445	c.20	1200-2000	**1600**
Mtsoli Basin*	Upper Onverwacht Gr, South Africa	***Buck Reef***	c.3451	17	1920-2750	**1900**
South Coongan Basin	Mt Ada-Duffer-Towers	***Shark Gully***	c.3464	25	3850	**3800**
North Coongan Basin	Mt Ada- Duffer	***Central Coppin Gap***	c.3465 – c. 3463	c.40	3000-4000	**3500**
Talga Basin*	North Star-Dresser	***North Pole Chert***	c. 3480	>10	1500-2000	**1700**
Coonterunah Basin*	Table Top-Coucal	***Table Top/Coucal***	>3530 - c.3500	22	2800	**2800**

***new basin names **location of VSC's in Fig. 5 (for names of basins and VSC's, and for numerical data other than in this article, see Nijman et al.2017)**

(1) five superposed shear planes: at locality 'r' in Fig. 12B, the crustal depths are: 2750 m for the combined shear planes I and II (separated from each other further eastwards), 2440 m (III), 2210 m (IV), and 1920 m (V); maximum crustal depths are measured at loc.'i';
(2) maximum thickness of 1950 m of the mafic-felsic volcanic rock sequence, measured vertically (i.e at right angles to the reference plane of BRC-Unit 4) through the back-tilted stratification at locality 'l', and of 630 m of the accumulated cherts of BRC-Units 1–4 (in the hanging wall at locality 'i'/ 'j');
(3) considerable westward (*i.e.* towards the basin centre) stratigraphic expansion of the BRC-Units 2–4 to over 1000 m, where shallow marine to inshore platform facies of the cherts interdigitate with iron-rich basin centre shale, tuff and some basalt (Fig. 13; Supplementary Fig. 13*).

The original geometry and dimensions in the restoration of Fig. 12B show the BR-VSC to be the most complete example of a volcano-sedimentary complex. Compared with the examples from the Pilbara, the BR-VSC is exceptional in showing (1) extreme back tilt, (2) a well-developed roll-over anticline with crestal unconformity, (3) facies change from near the basin margin in the east to the platform slope towards a remote basin centre in the west, (4) off-and-onlap relations within the chert (Supplementary Fig. 13*), (5) stepwise upward migration of the basal detachment surface (I-V) keeping pace with upward growth of the basin margin platform (BRC-Units 0–4), and (6) regularly spaced intrusion of TTG bodies along major growth faults.

*5.3. Remarks on the stratigraphic and paleogeographic position of the Buck Reef-**VSC***

The BR-VSC is situated in the north limb of the c. 3250 Ma, subvertical-plunging Onverwacht Anticline which bends the older part of the greenstone belt (inset figure in Fig. 12A). The BR stratigraphic interval can be traced eastwards around the anticlinal crest into the southeast limb of the anticline. There, Lowe and Byerly (2020) describe a sequence in the Komati River Gorge of 150 m felsic volcanic/volcanoclastic rocks (*their unit H6,* correlate with the lower two-thirds of the BR-VSC) and interpret its basin setting as deepening, stratigraphically upwards and sideways to the southwest, from subaerial to below wave base *(their figure 14)*. The felsic rocks are overlain by 300 m komatiite and (ultra)mafic tuff with two relatively thin units of black chert correlated with the BR Chert (*their unit K1)*. This observation creates an apparent contradiction with our interpretation in Section 5.1 of the BR-VSC as a west-facing basin margin prism, also with an increase of subaerial exposure to the east.

The apparent contradiction consists of the presence of isochronous basin margin sequences on either side of the hinge of the vertical Onverwacht Anticline, both with the deepening trend away from the hinge, at right angles to the fold axis. There are two options to resolve this:

1) Unfolding of the (sub-)vertical Onverwacht Anticline and back-rotation of the bedding to horizontal would bring the two sequences in a position of two oppositely oriented basin margins, comparable with the situation along the Warrawoona Lineament in the Pilbara (see Section 3.3). In that case, the basin separation, situated at the anticlinal hinge, coincided with a paleo-topographical (subaerial?) culmination where felsic volcanic activity was concentrated, directing felsic lava flows either side (cf. the basin model for the Pilbara in figure 9 of Nijman et al. 2017). Our observation that close to the axial plane of the Onverwacht Anticline (Fig. 12A, utmost righthand side) the TTG intrusions and sills of the BR-VSC connect with a conduit of felsic intrusions (with sidewards sills), ascending from deeper levels through the Hooggenoeg Fm, matches such a setting.
2) If, on the other hand, the axis of the Onverwacht Anticline would change from the observed subvertical position (exposed) into a subhorizontal position (now eroded away), the two deepening sequences might belong to the same west to southwest facing basin margin, *i.c.* of the Mtsoli Basin.

6. Discussion: Paleoarchean collapse structures compared with deformation in Phanerozoic basin margin prisms

Our examples of syndepositional gravitational deformation in Paleoarchean greenstone belts exhibit the full range of basin margin collapse features, listric growth fault arrays with visible linkage of extension and contraction, and megaslides (e.g. the Bergamina Unit). They occur in a setting of largely volcanic basins, superposed due to crustal oscillation (see definition in Section 1.2). This basin setting does imply active crustal-scale extension, though not in a plate-tectonic context, but in one probably unique for the Paleoarchean.

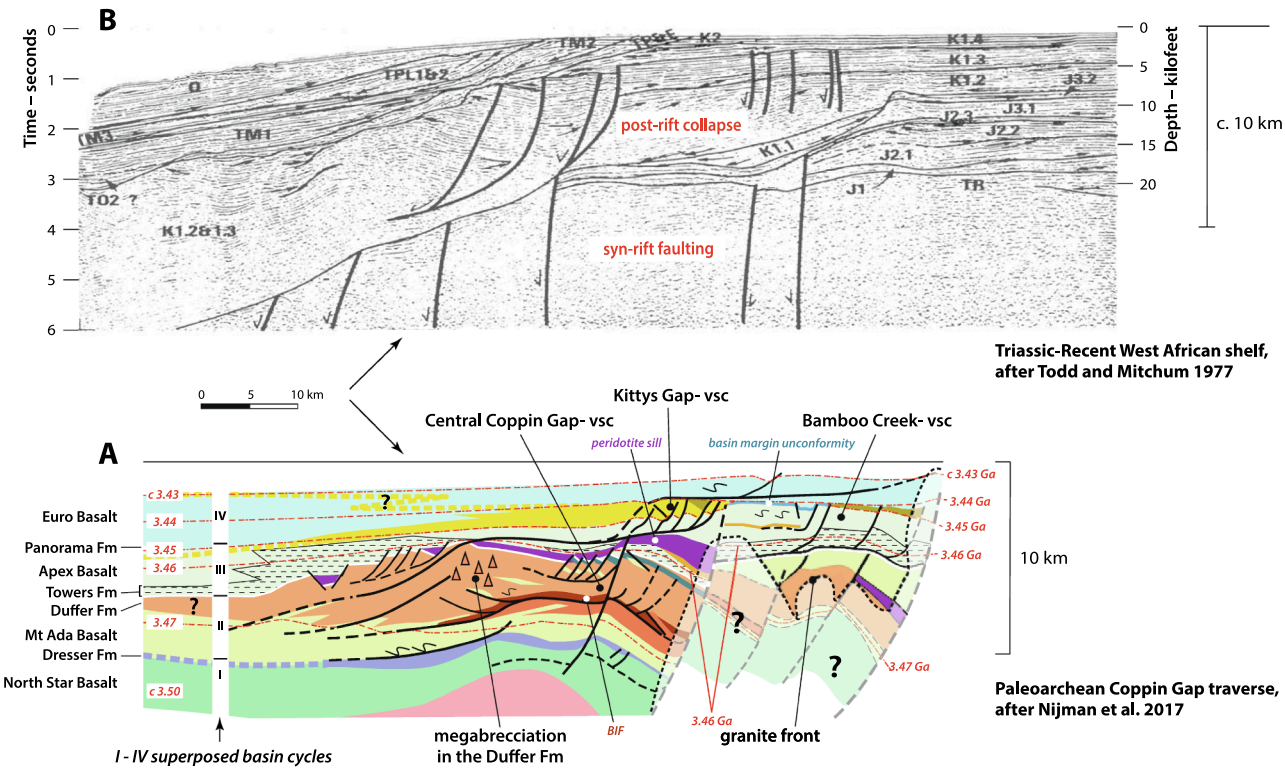

Fig. 14. Equal-scale comparison of architecture of (A) the reconstructed Paleoarchean basin margin in the Marble Bar greenstone belt (Marble Bar, Coppin Gap and Bamboo Creek Sectors) of the east Pilbara (from the traverse in Fig. 3c in Nijman et al. 2017) with (B) the West African Shelf (after Todd and Mitchum, AAPG©1977, reprinted by permission of the AAPG whose permission is required for further use). The basin cycles I – IV in figure A correspond with the basin fill sequences of, respectively, the Talga, (North) Coongan, (North) Salgash, and Kelly Basins of Table 1.

6.1. *Geometry and size of the Paleoarchean **VSC**'s*

The Buck Reef, Kittys Gap, Shark Gully, Witnell, and Central Coppin Gap-VSC's show the combination of extension at the rear and frontal contraction. In the Table Top - Coucal, Bamboo Creek, and North Pole-VSC's only extension is visible. The Bergamina Unit probably represents the base-of-slope accumulation of a partly collapsed basin margin. Their exposed lengths reach up to 40 km, while detachment depths range from c. 4000 to c.1000 m (Table 1).

6.2. *Is detachment depth a proxy for basin depth?*

The Bamboo Creek-Coppin Gap Sector of the Pilbara traverse of Fig. 14A remarkably resembles the seismic section of the northwestern African shelf (Fig. 14B) described by Todd and Mitchum (1977; Sheriff 1987), notwithstanding that the type of basin involved is completely different.

In passive margins, *post-rift* gravitational mass transport along slightly basinward dipping detachment planes, whether by normal fault arrays or as incoherent slump, is primarily facilitated by density difference between basin margin prism and sea water. We therefore assume detachment depth to be an important clue to the water depth, a still largely unknown parameter in Paleoarchean basin analysis. If a detachment plane below a normal fault array is situated along the base of a basin margin prism emerging *at* basin floor level, the distance from sea level (in our examples the top of the VSC) to the detachment plane, in other words the thickness of the VSC, matches basin depth (e.g. *figure 9e,f in* Peel 2014, *figure 4 in* Tamara et al. 2020). Because detachment planes can also emerge *above* the basin floor along the slope of the basin margin prism, the values given in Table 1 are *minimum* basin depth estimates. The table shows a depth range between 1000 and 3800 m for the basins listed. Such depths correspond remarkably well with those derived from depth-vesicularity relationships of pillow basalts in the Barberton Greenstone Belt: 2.4–4 km depth for the Hooggenoeg Fm, 1.7 km for the Kromberg Fm (cf. Furnes et al. 2011, 2013; De Wit et al. 2018, *p.647*).

The two arrows in the table suggest basin depth decreased over time in the Coonterunah/Talga and Salgash Basins. The maximum observed VSC sizes are those of the Shark Gully and Central Coppin Gap-VSC's. They correspond with estimated minimum water depths in the North and South Coongan Basins [5]of, respectively 3500 m and 3800 m. These large depth values are reached during the period of the most voluminous deposition of intermediate to felsic lava and volcanoclastic rocks of the Warrawoona Group, the Duffer Fm, around 3465 Ma ago. With the combination of maximum deepening and rapid build-up of the basin margin with lava and volcanoclastic sediment, one would expect the steepest and most unstable slopes, such as may have generated the Bergamina slide.

6.3. *The Bergamina avalanche event*

Does the Bergamina Unit fit in with other collapse structures found in VSC's of the Pilbara and Barberton?

According to Masson et al. (2006), the largest modern slides occur mainly in two settings, on open continental margins, like the West African Atlantic shelf margin, and on the flanks of oceanic islands. A quote from their article illustrates the dimensions and setting of these modern slides to be very similar to what we observe in the Bergamina Unit: *(their p. 2021; without their references) "a debris avalanche is …0.4 – 2 km thick*

[5] Because of basin separation along the Warrawoona Lineament, the Coongan Basin distinguished by Nijman et al. (2017) to the north of the lineament is now named *North* Coongan Basin, and its contemporary counterpart south of the lineament *South* Coongan Basin. A similar distinction has been made for the Salgash Basin.

with … a distal train of blocky debris. Each debris avalanche appears to be a single event, at least in terms of geological time, and some show evidence for rapid and energetic emplacement. ……..A typical Canary island debris avalanche is marked … by an erosive chute on the upper part of the submarine island slope and a pile of avalanche debris at the foot of the steepest island slope, usually at 3000–4000 m water depth,….has a volume of 50–200 km^3, covers an area of a few thousand km^2 and has a run-out of 50–100 km. Glide planes at the base of the land avalanche are typically up to 10° on the upper slope, decreasing to < 5° on the lower slope".

With up to 1 km-sized enclosed slabs and blocks, the Bergamina Unit should be classified as a mega-(debris-) avalanche. The preserved thickness reaches to just over 2 km in the Coonterunah S-sector (Fig. 11), an order of magnitude corresponding with the dimensions given by Masson et al. (2006) and appropriate to the estimated basin depths in Table 1.

Towards east, the underlying detachment cuts downwards into the stratigraphic column through the Double Bar Fm towards a level within the Coucal Fm. Although the Coonterunah outcrops are situated west of the Mulgandinnah Shear Zone, an eastward direction of the Bergamina mass displacement (Fig. 4D and 5) matches the (semi)-circular shape proposed for the superposed basins east of the shear zone (Nijman et al. 2017). The observation may limit the amount of strike-slip displacement along that fundamental fault.

Timing and stratigraphic position of the Bergamina Unit. Given the maximum available period of 30 Ma (3496–3466 Ma, see Section 4.3) for the emplacement of the Bergamina avalanche, and assuming sliding on such a large scale to have occurred during a phase of maximum rate of subsidence, deposition, and, as a consequence, margin instability, we suggested that the event likely occurred during deposition of the Duffer Fm. It would imply that the Bergamina tectono-stratigraphic unit should not be considered part of the Coonterunah Subgroup, but be linked to the Coongan Subgroup. In this context, the megabrecciation reported to occur in the Duffer Fm of the Coppin Gap Sector of the Marble Bar Belt (De Vries et al. 2006a; see also Fig. 14A) might represent a comparable collapse phenomenon on the opposite site of the same depositional basin.

6.4. Basin development

Fig. 14A illustrates that in the Coppin Gap Sector of the Marble Bar Belt the North Coongan Basin fill (cycle II: Mt Ada Basalt and Duffer Fm combined) reaches a maximum thickness of c. 5 km where, in the basin margin, intermediate felsic lavas and agglomerates of the Duffer Fm dominate over Mt Ada Basalt. Westwards, towards the basin centre, the ensemble is only c. 2 km thick and in the North Pole Dome the Duffer volcanic suite pinches out within the Mt Ada Basalt. The thickness difference of c. 3 km between the stratigraphic columns of margin and floor of the North Coongan Basin is of the same order as the depth estimate of c. 3.5 km in Table 1.

Previously, we (Nijman et al. 2004) explained the forming of the Buck Reef-VSC in South Africa as resulting from initial crustal uplift of a subaquatic pillow basalt plateau of unknown depth to near-emersion, followed by a subsidence back to pillow basalt depth. Sedimentation of the chert cap took place at about sea level during that transition, visible in off- and onlap facies relationships (Supplementary Fig. 13*). Lateral sedimentary facies shift does not solely depend on vertical tectonic movements but also on the rate of sediment supply and, in connection with open sea, on eustacy. Therefore, a change from regressive to transgressive facies in the capping chert formation does not need to exactly coincide with a change in vertical crustal movement. The stratigraphic position of this tipping point varies between VSC's: in the Kittys Gap-VSC (De Vries et al. 2010) and Table Top/Coucal-VSC (this article: Section 4.2) it lies along the top of the chert cap, instead of within the chert sequence as observed in the Buck Reef Chert.

Extension and opening of the system to bimodal volcanism we interpreted to have started during uplift above a relatively small *intra*crustal plume or hotspot. The deposition of the basin margin wedge and concurrent basin center-directed growth faulting and avalanching must have taken place during subsequent subsidence forming a large closed or semi-open basin as illustrated in Nijman et al. (2017).

Basin superposition in relation to vertical crustal oscillations, as proposed by us in 2017 for the area north of the Warrawoona Lineament (cf. Fig. 14A), is now also recognized south of the lineament in the superposition of the Shark Gully and Witnell-VSC's. The extremely reduced Panorama Fm in between these two VSC's, corresponds further eastwards with the well-developed Panorama Fm outcrops in the North Kelly-VSC.

7. Summary of results and main conclusions

(1) ***Volcano-sedimentary complexes (VSC's) with syndepositional collapse structures are recognized in addition to those previously reported in the eastern Pilbara.*** From oldest to youngest: the c. 3510 Ma Table Top/Coucal-VSC (Coonterunah Subgroup in the East Strelley Belt), the c. 3460 Ma Shark Gully-VSC (Coongan Subgroup in the Coongan Belt), the c. 3430 Ma North Kelly-VSC (Salgash Subgroup in the eastern Kelly Belt), and the c. 3320 Ma Witnell-VSC (Kelly Subgroup in the eastern Kelly Belt), all participating in the regional D1 phase of deformation.

(2) ***VSC-characteristics suggest a common depositional environment and underlying cause for deformation not unique for the Pilbara Craton.*** Where complete, the VSC's are composed of basalt, upwards transitional into felsic volcanic rocks and capped by zero-water depth sedimentary cherts. They are underlain by bedding (sub-)parallel detachment planes. The deformation is intraformational, syndepositional, gravitational, with a combination of arrays of proximal, mainly listric, normal faults, and distal thrusts at the toe. The full range of these structures occurs in the Buck Reef-VSC in the Barberton greenstone belt, South Africa, with which the VSC's of the Pilbara are compared.

(3) ***New observations in the c. 3.51 Ga Coonterunah Subgroup reveal a basin margin and slope architecture, with important eastward mass transport, matching with the previously proposed (semi)-circular geometry of superposed basins.*** The oldest volcanic sequence of the Pilbara has a multistorey architecture. The east-verging Table Top /Coucal-VSC is overlain by regularly bedded Double Bar Basalt, the ensemble truncated by an eastwards and downwards cutting detachment plane below a newly identified tectono-stratigraphic unit of chaotic internal structure, the Bergamina Unit. The east vergence of the Coonterunah Subgroup fits well with the (semi-)circular basin shape proposed for the area east of the Mulgandinnah Shear Zone (Shaw Structural Corridor), although its current position, west of it, must have been influenced by c. 2.95 Ga sinistral offset of unknown proportion along that fundamental fault zone.

(4) ***The Bergamina Unit is a base-of slope avalanche deposit possibly coeval with the Duffer Fm.*** The Bergamina Unit has the characteristics of a large avalanche, transported eastwards. Geochronological constraints dictate that this must have happened between c. 3496 and c. 3466 Ma. The extraordinary scale of its mass transport makes it plausible that the Bergamina avalanching took place during Duffer Fm/ Mt Ada Fm time, coeval with the forming of the North and South Coongan Basins. The stratigraphic position of the Bergamina Unit within the Coonterunah Subgroup therefore has to be reconsidered.

(5) ***The Warrawoona Lineament, an east–west trending, first-order, long-lived lithospheric-scale structure, served as a dividing line between two areas of basin formation.*** The transport direction indicated by the listric fault arrays in both the Kelly and Coongan Belts is approximately southwards, 180° opposed to those north of the lineament in the western Marble Bar Belt and North Pole Dome. Since the VSC's have basin margin characteristics, in

places accentuated by unconformities, it means that the Warrawoona Lineament, a proven east–west D2 transfer fault, already played a role during D1 as a separation between basins.

(6) ***Intrusions have exploited detachments and extensional faults of the VSC's, confirming the relative weakness and dilational orientation of these structures.*** Intrusions include: peridotite and komatiite bodies (North Kelly-, Shark Gully-, Central Coppin Gap-VSC), ultramafic dykes composed of harzburgite (Table Top/Coucal-VSC) and wehrlite (Buck Reef-VSC), as well as chert veins (e.g. North Kelly-, North Pole Chert- and Kittys Gap-VSC's), and porphyritic TTG bodies along major growth faults in the Buck Reef-VSC. Reactivation of detachments enhanced permeability; many host gold mineralization (Bergamina Unit, Shark Gully-VSC, Bamboo Creek Shear Zone).

(7) ***VSC-dimensions and orientations help constrain the reconstruction of basin shape and size. Collapse structures allow the determination of minimum basin depths ranging from 1000 to 3800 m.*** Minimum basin depths are calculated by measuring the distance between the VSC-top cherts deposited at zero water depth and the basal detachments at maximum depth, *i.e.* along the base of the basin margin prism emerging at basin floor level. This way, the greatest minimum depth of 3800 m is assigned to the North and South Coongan Basins hosting the Mt Ada/Duffer Fms, basins with a high subsidence rate, maximum deposition, and as a consequence, maximum basin margin instability. to which the Bergamina avalanche might be linked.

(8) ***The Paleoarchean basin setting appears to have been unique.*** Whereas the syndepositional deformation style of the VSC's is an architectural feature the Pilbara basins and the Buck Reef Chert have in common with Phanerozoic passive margins, the Archean context begs consideration of alternative scenarios for the underlying cause for basin development. These early basins, their shape, size and stacking, were more likely related to crustal oscillation above *intra*crustal hotspots, as proposed in Nijman et al. (2017). The relationship between supracrustal deformation and deformation observed in the deeper crustal shear zones within the oldest components of the granitoid complexes still demands attention.

CRediT authorship contribution statement

Wouter Nijman: Conceptualization, Visualization, Writing - original draft, Writing - review & editing. **Sjoukje T. de Vries:** Investigation, Resources, Writing – review & editing, Validation. **Armelle Kloppenburg:** Investigation, Resources, Writing – review & editing, Validation.

Declaration of Competing Interest

The authors declare that they have no known competing financial interests or personal relationships that could have appeared to influence the work reported in this paper.

Data availability

Data will be made available on request.

Acknowledgements

The study is part of the Earth's Earliest Basins (EEB) Project at Utrecht University, the Netherlands, through many years financially supported by the Dutch Dr Schürmann Foundation.

It could not have been completed without the efforts of many colleagues and students at Dutch Universities in the past, with special mention of the pioneer's work of Tanja Zegers in the 1990's. Our manuscript benefitted considerably from the meticulous way our colleagues Christoph Heubeck, Scott MacLennan, and Axel Hofmann reviewed the manuscript, for which we are very grateful indeed. We thank Mrs Margot Stoete of the Faculty of Geosciences at Utrecht University for the preparation and layout of the figures.

Appendix A. Supplementary material

Supplementary data to this article can be found online at https://doi.org/10.1016/j.precamres.2023.107121.

References

Allmendinger, R.W., Cardozo, N., Fisher, D., 2013. Structural Geology Algorithms: Vectors and Tensors. Cambridge University Press, 302 p.

Anqing, C., Chong, J., Zhanghua, L., Hongde, C., Shenglin, X., Keke, H., Sihan, H., 2013. Salt tectonics and Basin Evolution in the Gabon Coastal Basin, West Africa. J. Earth Sci. 24, 903–917. https://doi.org/10.1007/s12583-013-0383-5.

Bagas, L., Van Kranendonk, M.J., Pawley, M., 2003. Split Rock, W.A. Sheet 2854: Western Australia Geological Survey, 1:100 000 Geological Series.

Bagas, L., Beukenhorst, O., Hos, K., 2004a. Nullagine, W.A. Sheet 2954: Western Australia Geological Survey, 1:100 000 Geological Series.

Bagas, L., Van Kranendonk, M.J., Pawley, M., 2004b. Geology of the Split Rock 1:100 000 sheet: Western Australia Geological Survey, 1:100 000 Geological Series Explanatory Notes, 43 p.

Bagas, L. 2005. Geology of the Nullagine 1:100 000 sheet: Western Australia Geological Survey, 1:100 000 Geological Series Explanatory Notes, 33 p.

Bickle, M.J., Bettenay, L.F., Boultier, C.A., Groves, D.L., Morant, P., 1980. Horizontal tectonic interaction of an Archaean gneiss belt and greenstones, Pilbara block, Western Australia. Geology 8, 525–529. https://doi.org/10.1130/0091-7613(1980)8<525:HTIOAA>2.0.CO;2.

Boulter, C.A., Bickle, M.J., Gibson, B., Wright, R.K., 1987. Horizontal tectonics predating upper Gorge Creek Group sedimentation, Pilbara Block, Western Australia. Precambr. Res. 133, 241–258. https://doi.org/10.1016/0301-9268(87)90023-4.

Branney, M.J., Kokelaar, P., 1994. Volcanotectonic faulting, soft-state deformation and rheomorphism of tuffs during development of a piecemeal caldera, English Lake District. Geol. Soc. America Bulletin 106, 507–530. https://doi.org/10.1007/s004450050024.

Buick, R., Thornett, J.R., McNaughton, N.J., Smith, J.B., Barley, M.E., Savage, M., 1995. Record of an emergent continental crust ~3.5 billion years ago in the Pilbara Craton of Australia. Nature 375, 574–577. https://doi.org/10.1038/375574a0.

Buick, R., Brauhart, C.W., Morant, P., Thornett, J.R., Maniw, J.G., Archibald, N.J., Doepel, M.G., Fletcher, I.R., Pickard, J.B., Smith, J.B., Barley, M.E., McNaughton, M.G., Groves, N.J., 2002. Geochronology and stratigraphic relationships of the Sulphur Springs Group and Strelley Granite: a temporally distinct igneous province in the Archaean Pilbara Craton. Australia, Precambrian Research 114, 87–120. https://doi.org/10.1016/S0301-9268(01)00221-2.

Byerly, G.R., Lowe, D.R., Wooden, J.L., Xie, X., 2002. An Archaean impact layer from the Pilbara and Kaapvaal Cratons. Nature 297, 1325–1327. https://doi.org/10.1126/science.1073934.

Caruso, S., Van Kranendonk, M.J., Baumgartner, J., Fiorentini, L., Forster, M.A., 2021. The role of magmatic fluids in the ~3.48 Ga Dresser Caldera, Pilbara Craton: New insights from the geochemical investigation of hydrothermal alteration. Precambr. Res. 362, 106299 https://doi.org/10.1016/j.precamres.2021.106299.

Cramez, C., Jackson, M.P.A., 2000. Superposed deformation straddling the continental-oceanic transition in deep-water Angola. Mar. Pet. Geol. 17, 1095–1109. https://doi.org/10.1016/S0264-8172(00)00053-2.

Dann, J.C., 2000. The 3.5 Ga Komati Formation, Barberton Greenstone Belt, South Africa, Part I: New maps and magmatic architecture. S. Afr. J. Geol. 103, 47–68. https://doi.org/10.2113/103.1.47.

De Silva, S., Self, S., 2022. Capturing the extreme in volcanology: the case for the term "Supervolcano". Frontiers in Earth Science, https://doi.org/10.3389/feart.2022.859237.

De Vries, S.T., Nijman, W., Wijbrans, J.R., Nelson, D.R., 2006a. Stratigraphic continuity and early deformation of the central part of the Coppin Gap Greenstone Belt, Pilbara, Western Australia. Precambr. Res. 147, 1–27. https://doi.org/10.1016/j.precamres.2006.01.004.

De Vries, S.T., Nijman, W., Armstrong, R.A., 2006b. Growth-fault structure and stratigraphic architecture of the Buck Ridge volcano-sedimentary complex, upper Hooggenoeg formation, Barberton Greenstone Belt, South Africa. Precambr. Res. 149, 77–98. https://doi.org/10.1016/j.precamres.2006.04.005.

De Vries, S.T., Nijman, W., De Boer, P.L., 2010. Sedimentary geology of the Palaeoarchaean Buck Ridge (South Africa) and Kittys Gap (Western Australia) volcano-sedimentary complexes. Precambr. Res. 183, 749–769. https://doi.org/10.1016/j.precamres.2010.09.005.

De Wit, M.J., Furnes, H., Robins, B., 2011. Geology and tectonostratigraphy of the Onverwacht Suite, Barberton Greenstone Belt, South Africa. Precambr. Res. 186, 1–27. https://doi.org/10.1016/j.precamres.2010.12.007.

De Wit, M.J., Furnes, H., MacLennan, S., Doucour, M., Schoene, B., Weckmann, U., Martinez, U., Bowring, S., 2018. Paleoarchean bedrock lithologies across the Makhonjwa Mountains of South Africa and Swaziland linked to geochemical, magnetic and tectonic data reveal early plate tectonic genes flanking subduction margins. Geosci. Front. 9, 603–665. https://doi.org/10.1016/j.gsf.2017.10.005.

Dooley, T. P., Hudec, M. R., Pichel, L. M. and Jackson, M. P. A., 2020. The impact of base-salt relief on salt flow and suprasalt deformation patterns at the autochthonous,

paraautochthonous and allochthonous level: insights from physical models. In: McClay, K.R., Hammerstein, J.A. (Eds.), Passive Margins: Tectonics, Sedimentation and Magmatism. Geological Society, London, Special Publication 476, 287-316. https://doi.org/10.1144/SP476.13.

Dupré, S., Bertotti, G., Cloetingh, S., 2007. Tectonic history along the South Gabon Basin: Anomalous early post-rift subsidence. Mar. Pet. Geol. 24, 151–172. https://doi.org/10.1016/j.marpetgeo.2006.11.003.

Fernandez, O., Olaiz , A., Cascone, L., Hernandez, P., Pereira, A. de F., Tritlla, J., Ingles, M.,Aida, B., Pinto, I., Rocca, R., Sanders, C., Herrá, A., Tur, N., 2020. Geophysical evidence for breakup volcanism in the Angola and Gabon passive margins. Marine and Petroleum Geology, 116: 1-19/104330. https://doi.org/10.1016/j.marpetgeo.2020.104330.

Fisher, R., Gerya, T.V., 2016. Early Earth plume-lid tectonics: A high-resolution 3D numerical modelling approach. J. Geodyn. 100, 198–214. https://doi.org/10.1016/j.jog.2016.03.004.

Furnes, H., de Wit, M., Robins, B., Sandstå, N.R., 2011. Volcanic evolution of the upper Onverwacht suite, Barberton Greenstone Belt, South Africa. Precambr. Res. 186, 28–50. https://doi.org/10.1016/j.precamres.2010.11.002.

Furnes, H., de Wit, M.J., Robins, B., 2013. A review of new interpretations of the tectono-stratigraphy, geochemistry and evolution of the Onverwacht Suite, Barberton Greenstone Belt, South Africa. Gondw. Res. 23, 403–428. https://doi.org/10.1016/j.gr.2012.05.007.

Gibbs, A.D., 1984. Structural evolution of extensional basin margins. J. Geol. Soc. (Lond.) 141, 609–620. https://doi.org/10.1144/gsjgs.141.4.0609.

Glikson, A.Y., Hickman, A.H., Evans, N.J., Kirkland, C.L., Park, J.-W., Rapp, R., Romano, S., 2016. A new 3.46 Ga asteroid impact ejecta unit at Marble Bar, Pilbara Craton, Western Australia: A petrological, microprobe and laser ablation ICPMS study. Precambr. Res. 279, 103–122. https://doi.org/10.1016/j.precamres.2016.04.003.

Glikson, A.Y., Vickers, J., 2010. Asteroid impact connections of crustal evolution Australian. J. Earth Sciences 57, 79–95. https://doi.org/10.1080/08120090903416211.

Green, M.G., Sylvester, P.J., Buick, R., 2000. Growth and recycling of early Archaean continental crust: geochemical evidence from the Coonterunah and Warrawoona Groups, Pilbara Craton, Australia. Tectonophysics 322, 69–88. https://doi.org/10.1016/S0040-1951(00)00058-5.

Grey, K., Clarke, J.D.A., Hickman, A.H., 2012. The proposed Dawn of Life Geotourism Trail, Marble Bar, Pilbara Craton, Western Australia – geology and evidence for early life. GSWA. Record 2012/9, 27 p.

Hamilton, W.B., 2019. Toward a myth-free geodynamic history of Earth and its neighbors. Earth Sci. Rev. 198, 102905 https://doi.org/10.1016/j.earscirev.2019.102905.

Hamilton, W.B., 2007. Earth's first two billion years – The era of internally mobile crust. In: Hatcher, Jr.,R.D., Carlson, M.P., McBride, J.H.,Martínez Catalán, J.R., 4-D Framework of Continental Crust. Memoir of the Geological Society of America, 200, 233-296. https://doi.org/10.1130/2007.1200(13).

Hickman, A.H., 2008. Regional review of the 3426–3350 Ma Strelley Pool Formation. Pilbara Craton, Western Australia, GSWA Record 2008 (15), 1–27.

Hickman, A.H., 2011. Pilbara Supergroup of the East Pilbara Terrane, Pilbara Craton: Updated lithostratigraphy and comments on the influence of vertical tectonics. GSWA Annual Review, 2009–2010: 50–59.

Hickman A.H., Van Kranendonk, M.J., 2008. Marble Bar, W.A. Sheet 2955, Western Australian Geological Survey 1:100 000 Geological Series.

Hickman, A.H. 2012. North Shaw, W.A. Sheet 2755. 2nd edn. Western Australian Geological Survey 1:100 000 Geological Series, Perth.

Hickman, A.H., 2021. East Pilbara Craton: a record of one billion years in the growth of Archean continental crust: Geological Survey of Western Australia, Report 143, 187p.

Hodgson, N., Rodriguez, K., 2017. Shelf stability and mantle convection on Africa's passive margins (Part 1). First Break 35, 93–97. https://doi.org/10.3997/1365-2397.35.3.87567.

Hooper, R.J., Fitzsimmons, R.J., Grant, N., Vandeville, B.C., 2002. The role of deformation in controlling depositional patterns in the south-central Niger Delta, West Africa. J. Struct. Geol. 24, 847–859. https://doi.org/10.1016/S0191-8141(01)00122-5.

Imber, J., Childs, C., Nell, P.A.R., Walsh, J.J., Hodgetts, D., Flint, S., 2003. Hanging wall fault kinematics and footwall collapse in listric growth fault systems. J. Struct. Geol. 25, 197–208. https://doi.org/10.1016/S0191-8141(02)00034-2.

Jarrige, J.-J., 1992. Variation in extensional fault geometry related to detachment surfaces within sedimentary sequences and basement. Tectonophysics 215, 161–166. https://doi.org/10.1016/0040-1951(92)90079-L.

Kloppenburg, A., White, S.H., Zegers, T.E., 2001. Structural evolution of the Warrawoona Greenstone Belt and adjoining granitoid complexes, Pilbara Craton, Australia: implications for Archaean tectonic processes. Precambr. Res. 112, 107–147. https://doi.org/10.1016/S0301-9268(01)00172-3.

Kloppenburg, A., 2003. Structural evolution of the Marble Bar Domain, Pilbara granite-greenstone terrain, Australia: The role of Archaean mid- crustal detachments (PhD thesis Utrecht University, the Netherlands). Geologica Ultraiectina, 237, 256 p.

Ledevin, M., Arndt, N., Chauvel, C., Jaillard, E., Simionovici, A., 2019. The sedimentary origin of black and white banded cherts of the Buck Reef, Barberton. South Africa. Geosciences 9, 424. https://doi.org/10.3390/geosciences 9100424.

Lowe, D.H., 1983. Restricted shallow-water sedimentation of early Archean stromatolitic and evaporitic strata of the Strelley Pool Chert, Pilbara Block, Western Australia. Precambr. Res. 19, 239–283. https://doi.org/10.1016/0301-9268(83)90016-5.

Lowe, D.R., Byerly, G.R., 2020. The non-glacial and non-cratonic origin of an early Archean felsic volcanoclastic unit, Barberton Greenstone Belt, South Africa. Precambrian Research, 341,105647. https://doi.org/10.1016/j.precamres.2020.105647.

Lowe, D.R., Byerly, G.R., 1999. Geologic Evolution of the Barberton Greenstone Belt, South Africa. Geol. Soc. Am. Spec. Pap. 329, 319 p. https://doi.org/10.1130/SPE329.

Lowe, D.R., Byerly, G.R., Heubeck, C., 2012. Geologic map of the West-Central Barberton Greenstone Belt, South Africa, Scale 1:25 000. Geological Society of America map and Chart Series, 103.

Mandl, G. and Crans, W., 1981. Gravitational gliding in deltas. In: K.R. McCLay and N.J. Price (Editors), Thrust and Nappe Tectonics. Geol. Soc. London Spec. Publ., 82: 41-54. https://doi.org/10.1144/GSL.SP.1981.009.01.05.

Marton, L.G., Tari, G.C., Lehmann, C.T., 2000. Evolution of the Angolan passive margin, West Africa, with emphasis on post-salt structural styles. In: Mohriak, W., Talwani, M. (Eds.), Atlantic Rifts and Continental Margins. American Geophysical Union Geophysical Monograph, 115, p. 129–149. https://doi.org/10.1029/GM115p0129.

Masson, D.G., Harbitz, C.B., Wynn, R.B., Pedersen, G., Løvholt, F., 2006. Submarine landslides: processes, triggers and hazard prediction. Philos. Trans. Roy. Soc. A 364, 2009–2039. https://doi.org/10.1098/rsta.2006.1810.

Mauduit, T., Brun, J.P., 1998. Growth fault/rollover systems: Birth, growth and decay. Journal of Geophysical Research, 103, 18.119-18.136. https://doi.org/10.1029/97JB02484.

McClay, K.R., Hammerstein, J.A., 2020. Passive Margins: Tectonics, Sedimentation and Magmatism. Geological Society, London, Special Publication 476, 447 p. [ISBN-13 : 978-1786203854].

McClay, K.R., Scott, A.D., 1991. Experimental models of hangingwall deformation in ramp-flat listric extensional fault systems. Tectonophysics 188, 85–96. https://doi.org/10.1016/0040-1951(91)90316-K.

Nelson, D.R., 2002. Compilation of Geochronology Data, 2001. GSWA Record 2002/2, 282 p.

Nijman, W., De Vries, S.T., 2004. Early Archaean crustal collapse structures and sedimentary basin dynamics. In: Eriksson, P.G., Altermann, W., Nelson, D.R., Mueller, W.U., Catuneanu, O. (Eds.), The Precambrian Earth: Tempos and Events. Developments in Precambrian Geology, Elsevier, 12, 139-155.

Nijman, W., De Vries, S.T., 2005. Geological map of the Lower Archaean Buck Ridge volcano-sedimentary complex, Barberton Greenstone Belt, Republic of South Africa. 3 Map sheets and Explanatory Notes. Faculty of Geosciences, Utrecht University, the Netherlands. ISBN: 978-90-5744-153-0 [available from: Utrecht University, Library Repository (Narcis), and via Researchgate].

Nijman, W., Willigers, B.J.A., Krikke, A., 1998/99b. Tensile and compressive growth structures: relation between sedimentation, deformation and granite intrusion in the Archaean Coppin Gap Greenstone belt, Eastern Pilbara, Western Australia. Precambr. Res. 95, 277–302 (erratum re-edition of Precambr. Res. 88, 83–107, 1998). https://doi.org/10.1016/S0301-9268(99)00013-3 (first edition: https://doi.org/10.1016/S0301-9268(97)00065-X).

Nijman, W., De Bruijne, C.H. & Valkering, M.E. 1998/99a. Growth fault control of Early Archaean cherts, barite mounds and chert-barite veins, North Pole Dome, Eastern Pilbara, Western Australia. Precambr. Res. 95, 247–274 (erratum re-edition of Precambr. Res. 88, 25–52, 1998). https://doi.org/10.1016/S0301-9268(99)00014-5 (first edition: https://doi.org/10.1016/S0301-9268(97)00062-4).

Nijman, W., Kloppenburg, A., De Vries, S.T., 2017. Archaean basin margin geology and crustal evolution: an East Pilbara traverse. with supplementary figures. J. Geol. Society, London 174, 1090–1112 http://dspace.library.uu.nl/handle/1874/357294.

Oliveira, M.J., Santarem, P., J.R.Moraes, A., Zalán, P.V., Caldeira, J.L., Tanaka, A., Trosdtorf Junior, I., 2012. Linked extensional-compressional tectonics in gravitational systems in the equatorial margin of Brazil. In: Gao, D. (Ed.), Tectonics and Sedimentation: Implications for Petroleum Systems. AAPG Memoirs 100, 159178. https://doi.org/10.1306/13351552M1003532.

Olson, J.R., Söderlund, U., Klausen, M.B., Ernst, R.E., 2010. U-Pb baddeleyite ages linking major Archean dyke swarms to volcanic-rift forming events in the Kaapvaal craton (South Africa), and a precise age for the Bushveld Complex. Precambr. Res. 183, 490–500. https://doi.org/10.1016/j.precamres.2010.07.009.

Peel, F.J., 2014. The engines of gravity-driven movement on passive margins: Quantifying the relative contribution of spreading vs. gravity sliding mechanisms. Tectonophysics 623, 126–142. https://doi.org/10.1016/j.tecto.2014.06.023.

Restrepo-Pace, P. A. 2020. 'Ductile v. Brittle' – Alternative structural interpretations for the Niger Delta. In: McClay, K.R., Hammerstein, J.A., (Eds.) Passive Margins: Tectonics, Sedimentation and Magmatism. Geological Society, London, Special Publication 476, 193-204. https://doi.org/10.1144/SP476.2.

Rowan, M.C., Peel, F.J., Vendeville, B.C., Gaullier, V., 2012. Salt tectonics at passive margins: Geology versus models – Discussion. Mar. Pet. Geol. 37, 184–194. https://doi.org/10.1016/j.marpetgeo.2012.04.007.

Sheriff, R.G., 1987. Passive Margins: Interpretation of West Africa Line C. In: A. W. Bally (Ed.), Atlas of Seismic Stratigraphy, AAPG Studies in Geology 27, vol. 2, pp. 37-44.

Smithies, R.H., Champion, D.C., Van Kranendonk, M.J., 2007. The oldest well preserved volcanic rocks on Earth: Geochemical clues to the early evolution of the Pilbara Supergroup and implications for the growth of a Paleoarchean continent. In: M.J. Van Kranendonk, V.C. Bennett, R.H. Smithies (Eds.), Earth's oldest rocks. Developments in Precambrian Geology, 15, 339–367. https://doi.org/10.1016/S0166-2635(07)15042-8.

Tamara, J., McClay, K.R., Hodgson, N., 2020. Crustal structure of the central sector of the NE Brazilian equatorial margin. In: McClay, K.R., Hammerstein, J.A., (Eds.) Passive Margins: Tectonics, Sedimentation and Magmatism. Geological Society, London, Special Publication 476: 163-191. https://doi.org/10.1144/SP476-2019-54.

Tice, M.M., Lowe, D.R., 2006. The origin of carbonaceous matter in pre-3.0 Ga greenstone terrains: A review and new evidence from the 3.42 Ga Buck Reef Chert. Earth Sci. Rev. 76, 259–300. https://doi.org/10.1016/j.earscirev.2006.03.003.

Todd, R.E., Mitchum Jr., R.M., 1977. Seismic Stratigraphy and Global Changes of Sea Level, Part 8: Identification of Upper Triassic, Jurassic, and Lower Cretaceous Seismic Sequences in Gulf of Mexico and Offshore West Africa. AAPG Mem. 26, 145–163. https://doi.org/10.1306/M26490C10.

Van Kranendonk, M.J., 2006. Volcanic degassing, hydrothermal circulation and the flourishing of early life on Earth: A review of the evidence from c. 3490–3240 Ma rocks of the Pilbara Supergroup, Pilbara Craton, Western Australia. Earth-Science Rev. 74, 197–240. https://doi.org/10.1016/j.earscirev.2005.09.005.

Van Kranendonk, M.J., 2008. Structural geology of the central part of the Lalla Rookh – Western Shaw structural corridor, Pilbara Craton, Western Australia. Geological Survey of Western Australia, Report 103, 29 p.

Van Kranendonk, M.J., McGuinness, S., Bodorkos, S., Hickman, A.H., 2012. Carlindie, W. A. Sheet 2756 (2nd ed.), Western Australian Geological Survey 1:100 000 Geological Series.

Van Kranendonk, M.J., Hickman, A.H., Smithies, R.H., Williams, I.R., Bagas, L., Farrell, T.R., 2006. Revised lithostratigraphy of Archean supracrustal and intrusive rocks in the northern Pilbara Craton, Western Australia. Geological Survey of Western Australia, Record 2006 (15), 57 p.

Van Kranendonk, M.J., Morant, P., 1998. Revised Archaean stratigraphy of the North Shaw 1:100 000 sheet, Pilbara Craton. Western Australia Geological Survey, Annual Review 1997–98, 55–62.

Van Kranendonk, M.J., Hickman, A.H., Williams, I.R., Nijman, W., 2001. Archaean geology of the East Pilbara granite-greenstone terrane, Western Australia – A field guide. Geological Survey of Western Australia, Record 2001 (9), 134 p.

Van Kranendonk, M.J., 1999. North Shaw, W.A. Sheet 2755, (1st ed.). Western Australian Geological Survey 1:100 000 Geological Series.

Van Kranendonk, M. J., 2000. Geology of the North Shaw 1:100 000 Sheet. Geological Survey of Western Australia (GSWA) 1:100 000 Geological Series Explanatory Notes, Perth, 68 p.

Wacey, D., McLoughlin, N., Stoakes, C.A., Kilburn, M.R., Green, O.R., Brasier, M.D., 2010. The 3426–3350 Ma Strelley Pool formation in the East Strelley greenstone belt – A field and petrographic guide. Geological Survey of Western Australia, Record 2010 (10), 64 p.

Westall, F., De Vries, S.T., Nijman, W., Rouchon, V., Orberger, B., Pearson, V., Watson, J., Verchovsky, A., Wright, I., Rouzaud, J.-N., Marchesini, D., Severine, A., 2006. The 3446 Ga "Kitty's Gap Chert", an early Archean microbial ecosystem. In: Reimold, W. U., Gibson, R.L., Processes on the Early Earth. Geological Society of America, Special Paper 405: 105-131. https://doi.org/10.1130/2006.2405(07).

Williams, I.R., Bagas, L., 2004. Mount Edgar, W.A. Sheet 2955, Western Australian Geological Survey 1:100 000 Geological Series.

Williams, I.R., Bagas, L., Boas, I.H., 2007. Geology of the Mount Edgar 1:100 000 Sheet. Geological Survey of Western Australia (GSWA) 1:100 000 Geological Series Explanatory Notes, Perth, 62 p.

Zegers, T.E., White, S.H., De Keijzer, M., Dirks, P., 1996. Extensional structures during the deposition of the 3460 Ma Warrawoona Group in the eastern Pilbara Craton, Western Australia. Precambr. Res. 80, 89–105. https://doi.org/10.1016/S0301-9268(96)00007-1.

Zegers, T.E., De Keijzer, M., Passchier, C.W., White, S.H., 1998. The Mulgandinnah shear zone: an Archean crustal-scale strike-slip zone, eastern Pilbara, Western Australia. Precambr. Res. 88, 233–248. https://doi.org/10.1016/S0301-9268(97)00070-3.

Zegers, T.E., 1996. Structural, kinematic and metallogenic evolution of selected domains of the Pilbara granite-greenstone terrain; implications for mid-Archean tectonic regimes. (PhD thesis, Utrecht University, The Netherlands). Geologica Ultraiectina, 146, 208 p.